Materials Today Communications 35 (2023) 106159

Contents lists available at ScienceDirect

Materials Today Communications

journal homepage: www.elsevier.com/locate/mtcomm

Identification of the extended standard linear solid material model by means of experimental dynamical measurements

Stefano Amadori [a,*], Giuseppe Catania [b]

[a] Ciri-Mam, University of Bologna, Viale Risorgimento 2, 40136 Bologna (BO), Italy
[b] DIN-Department of Industrial Engineering, Ciri-Mam, University of Bologna, Viale Risorgimento 2, 40136 Bologna (BO), Italy

ARTICLE INFO

Keywords:
Fractional derivative model
Extended SLS model
Hysteretic model
Non-parametric identification

ABSTRACT

A novel algebraic procedure for the non-parametric identification of the material model by means of dynamical test measurements is proposed. An extended Standard Linear Solid (SLS) material model is taken into account to model the material linear visco-elastic behavior. It consists of the series arrangement of fractional Kelvin model elements adopting real parameters and integer and non-integer order time differential operators, and of hysteretic Kelvin model elements adopting complex parameters and integer order time differential operators. Hysteretic Kelvin model elements are introduced to take account of the material hysteretic behavior. The material $E(j{\cdot}\omega)$ complex modulus, is analytically modeled as the ratio of pseudo polynomials (non-integer power terms) in the $j{\cdot}\omega$ Fourier variable. A multi-step, iterative, material model identification technique is here proposed to identify the unknown polynomial coefficients and the non-integer exponent values starting from $E(j{\cdot}\omega)$ material discrete estimates from input-output dynamical measurements made on a beam specimen at different ω frequency values. Computational, nonphysical SLS elements resulting from the application of the identification procedure can be found and eliminated, so that a low order optimal model result. Some results obtained by applying the proposed identification technique with real experimental measurements are shown and discussed.

1. Introduction

The material uniaxial σ stress v/s ε strain unknown frequency function, $\widehat{\sigma}/\widehat{\varepsilon} = E(j{\cdot}\omega)$, where $\widehat{()}$ refers to the Fourier transform operator, $j = \sqrt{-1}$, and ω is the circular frequency, can be experimentally estimated by means of input-output measurements made on a beam specimen in stationary forced vibration conditions and in low strain response conditions. Dynamic Mechanical Analysis (DMA) test systems are generally used for this task [1], and homogeneous, uniform beam specimens made with the material under study, excited in a flexural, tension or compression experimental set-up under known boundary conditions (*BC*) at the beam ends, are generally taken into account. The beam is harmonically excited at a fixed ω frequency value by means of a f force in correspondence of a fixed axial position. Both the $|f|$ amplitude, the $|u|$ displacement amplitude in correspondence of the same or a different axial position, and the displacement $\Delta\varphi/\omega$ time delay with respect to the excitation are measured, so that the complex $\widehat{u}/\widehat{f} = (|\widehat{u}|/|\widehat{f}|){\cdot}\exp(-j{\cdot}\Delta\varphi)$ frequency response (FRF) ratio can be estimated from measurements made at different ω values. From the standard beam linear theory of elasticity $\widehat{u}/\widehat{f} = \widehat{u}/\widehat{f}(E(j{\cdot}\omega),\ \omega,\ \text{geometry},\ \text{density},\ BC)$ [2], so that the $E(j{\cdot}\omega) = E(\widehat{u}/\widehat{f}(\omega))$ can be estimated from $\widehat{u}/\widehat{f}(j\omega)$ measured values. The contribution of the beam inertial forces and of the test instrument elasto-inertial response can also be taken into account, in order to increase the accuracy of the $E(j{\cdot}\omega)$ estimate, and some techniques are known [3,4]. The resulting material $E(j{\cdot}\omega)$ estimate obtained from a specific DMA test specimen is expected to be consistent and can be used to simulate the response of any structure under linearity assumptions. Under multiaxial stress-strain conditions, e.g., when solid or thin-walled shell structures are taken into account, other material parameters should be experimentally estimated, such as the $G(j{\cdot}\omega)$ share complex modulus from within dynamical measurements in uniaxial shear conditions. Nevertheless, in some conditions, i.e., when isotropic materials associated to a stationary Poisson coefficient with respect to frequency are considered, the material $E(j{\cdot}\omega)$ complex modulus only, fully describes the material multiaxial $\boldsymbol{\sigma} = \mathbf{D}{\cdot}\boldsymbol{\varepsilon}$ stress v/s strain relationship [5,6].

While $E(j{\cdot}\omega_k),\quad \omega_k \in \Omega = [\omega_1, \ldots, \omega_{N_x}]$ estimated discrete values can be used as the effective material model in the frequency domain for

* Corresponding author.
E-mail addresses: stefano.amadori4@unibo.it (S. Amadori), giuseppe.catania@unibo.it (G. Catania).

https://doi.org/10.1016/j.mtcomm.2023.106159
Received 6 March 2023; Received in revised form 21 April 2023; Accepted 7 May 2023
Available online 9 May 2023

some engineering tasks, a continuous $E(j{\cdot}\omega)$ model is generally needed in most engineering applications, e.g. when the relaxation material response has to be obtained from $E(j{\cdot}\omega)$ or when such discrete material model needs to be interpolated or extrapolated outside the Ω frequency measurement range. Many different $E(j{\cdot}\omega)$ continuous models can be found in the scientific literature. A classical approach yields the SLS model [7,8] consisting in N (N referring to the SLS model order) linear viscoelastic Kelvin elements arranged in series [5,9–11]. Since most basic low order models, consisting of $N \leq 2$ elements, such as the Maxwell, Kelvin, Zener SLS models, show limitations in describing the material dynamical behavior when a wide frequency range is taken into account, such basic models are generally not consistent when used to model both the stress-strain relaxation and the high frequency vibrational behavior of a structure made with the material under study. The basic SLS material model parameters that result in an optimal fit for a mid to high frequency vibrational process, result in a poor fit for a quasi-static dynamical process, e.g., when stress or strain relaxation responses are considered [1,3]. The behavior associated with slow and fast dynamic response cannot generally be modeled by means of SLS low order models. More detailed examples of such limitation are presented in Section 2. It also appears that SLS low order models cannot accurately model some composite or functionally graded materials (FGM) even in a restricted frequency range. High order SLS models consisting of $N > 2$ real Kelvin elements [1,5,7] can be used to deal with the previously outlined limitations. It appears that, by increasing N, the dynamic behavior of some structures made of composite or functionally graded materials can be effectively modeled [4,5,7,11–14].

It can be found that the $E^{-1}(j{\cdot}\omega)$ strain to stress ratio model derived from assuming real Kelvin elements (real, positive elastic and viscous parameters) can be expressed as the ratio of two rational polynomial functions with real coefficients in the complex $j{\cdot}\omega$ variable [3,4,15]. It can also be found [3] that, in partial fraction form, real negative poles and real positive residues result.

Nevertheless, it was found by the authors of this paper [3] that continuous $E^{-1}(j{\cdot}\omega)$ resulting from an extended low order SLS model associated to complex poles and residues may better fit $E^{-1}(j{\cdot}\omega_k)$ experimentally estimated values from testing of non-conventional materials such as composite and FGM materials. SLS models associated to complex poles and residues include hysteretic Kelvin elements, a hysteretic Kelvin element being a generalization of the standard Kelvin element where both the elastic and the viscous parameters are associated with complex values. The authors of this paper used this approach in some previous works [16] to model the internal shear friction in multi-layer composite beam specimens. It must be taken into account that a hysteretic model is not physical since it is not causal (non-null strain response to a Dirac stress impulse at $t < 0$ typically results), the imaginary part of the time response to a step input and of the free vibrational response are not null since $E(j{\cdot}\omega) \neq (E(-j{\cdot}\omega))^{*}$, where $()^{*}$ is the complex conjugate operator. It results that the hysteretic model cannot be used to simulate a quasi-stationary behavior ($j{\cdot}\omega{\to}0$), nor the free vibrational response of a structure but can be effectively used to model the dynamical response of the same structure under a forced vibrational excitation as it occurs in most engineering applications [17–23].

Material models employing fractional derivatives were investigated in many works [6,24–30]. It was found that the relaxation behavior of some materials, such as most polymers [31], can be optimally modelled by means of a low order generalized SLS model employing fractional derivative operators. As a result, a reduced number of elements is generally needed to accurately fit experimental measurements in both quasi-static (relaxation) and high frequency vibrational behavior with respect to the SLS approach. In Section 2 the critical comparison between the expected behavior of a slender beam made of a material following a fractional SLS material model and of a SLS material model is shown.

Numerical parametric identification of the parameters of a SLS model is a non-trivial task and some techniques were proposed in the past [32–36]. It should be outlined that the model identification task associated to $N > 2$ may be difficult from the experimental and computational standpoint, since the resulting high number of unknown parameters to be identified may require many test measurements in an extended Ω range and an ill conditioned system of nonlinear equations may result in the identification problem.

A non-parametric approach, based on the application of the Levy's technique [37], was recently proposed by these authors [4], making it possible to identify the optimal N order and the physical parameters associated to each SLS element, starting from $E(j{\cdot}\omega_k), \omega_k \in [\omega_1, \ldots, \omega_{N_x}]$ experimentally estimated values. Nevertheless, such technique cannot be applied to identify an extended SLS model including fractional and hysteretic elements. The identification of the parameters of an extended SLS model was mainly dealt with nonlinear optimization techniques in the past [38–45]. Nevertheless, since the accuracy of the result strongly depends on the choice of the starting set of the unknown model parameter values needed by the optimization algorithm, the effectiveness of this approach is low and its application is practically limited to the identification of $N \leq 2$ low order models [43,44,46].

The $E^{-1}(j{\cdot}\omega)$ strain to stress ratio model associated to a fractional SLS model can be expressed as the ratio of pseudo polynomials (non-integer power terms) in the $j{\cdot}\omega$ Fourier variable or the ratio of two polynomials in the $(j{\cdot}\omega)^{1/D}$, $D \in \mathbb{N}$ [47], where the denominator polynomial order is greater or at least equal to the numerator polynomial order. The parametric identification of the coefficients of $E^{-1}(j{\cdot}\omega)$ polynomials was proposed in the past by some researchers. A technique based on the Levy's approach was proposed by Kapp [47], but D and the order of the two polynomials is required to be known in advance. The optimal solution is obtained by least squares minimization of the error associated with a system of linear equations but the optimal model size does not result from the application of this approach, so this technique cannot be applied *as-is* to identify an extended SLS model.

A material iterative model identification procedure is here proposed. The number of both the fractional and hysteretic Kelvin elements, and the derivative non-integer order associated to any fractional element constituting the extended SLS model to be identified is not a priori assumed, meaning that a non-parametric identification procedure results. The parameters of the fractional and hysteretic Kelvin elements can be identified as well. The procedure makes it possible to eliminate computational, non-physical results, mainly due to the experimental noise in input data and to the signal processing numerical noise, so that a minimal model order is generally expected to result.

Some application test cases are discussed in detail to show the effectiveness of the proposed technique.

2. Dynamical behavior of structures made of materials following SLS and fractional SLS models

A Kelvin model, corresponding to a $N = 1$ SLS model, is first taken into account, its constitutive equation being:

$$\sigma(t) = E_0 \cdot \left(\varepsilon(t) + \frac{\beta}{E_0} \cdot \dot{\varepsilon}(t) \right), \tag{1}$$

where $\dot{()}$ is the time derivative operator, material σ and ε refer to stress and strain in uni-axial conditions, E_0, β refer to the elastic and viscous Kelvin model parameters. By assuming $\sigma(t \geq 0) = \sigma_0$, $\sigma(t < 0) = \varepsilon(t < 0) = 0$, the creep relaxation response $\varepsilon(t)$ exponentially converges to $\varepsilon(t = \infty) = \sigma_0/E_0$, with time constant β/E_0 [5]. By assuming that the τ_c creep relaxation time satisfies the following condition:

$$\varepsilon(t = \tau_c) = \frac{\sigma_0}{E_0} \cdot \left(1 - exp\left(-\tau_c \cdot \frac{E_0}{\beta} \right) \right) = 95\% \cdot \varepsilon(t = \infty) = 0.95 \cdot \frac{\sigma_0}{E_0}, \tag{2}$$

Table 1
HDPE beam specimen data.

Density (kg/m^3)	Length (m)	Width (m)	Thickness (m)	E_0 (Pa)
945	1.65	0.04	0.011	$1.08\bullet10^9$

Table 2
Reference SLS model example cases.

Case	Model parameters			
SLS	N	α_i	E_i [Pa]	β_i [Pa•s$^{\alpha}$]
(A)	1	1	$1.08\bullet10^9$	$3.60\bullet10^8$
(B)	2	1	$5.40\bullet10^9$	$1.95\bullet10^{11}$
		1	$2.80\bullet10^{10}$	$8.35\bullet10^{10}$
(C)	2	1	$1.02\bullet10^9$	$3.97\bullet10^{10}$
		1	$1.05\bullet10^{10}$	$1.38\bullet10^5$
Fractional SLS	N	α_i	E_i [Pa]	β_i [Pa•s$^{\alpha}$]
(D)	1	0.9	$1.08\bullet10^9$	$1.70\bullet10^{10}$
(E)	1	0.5	$1.08\bullet10^9$	$9.75\bullet10^8$
(F)	1	0.2	$1.08\bullet10^9$	$1.85\bullet10^8$
(G)	1	0.1	$1.08\bullet10^9$	$1.45\bullet10^8$
(H)	2	0.1	$2.16\bullet10^9$	$1.10\bullet10^8$
		0.2	$2.16\bullet10^9$	$6.20\bullet10^8$

it follows that β viscous parameter satisfies Eq. (3):

$$\beta = \frac{\tau_c \cdot E_0}{\ln(20)} \simeq \frac{\tau_c \cdot E_0}{3}. \tag{3}$$

It can be shown [3,5] that the free response of a uniform homogeneous beam structure, whose material model follows Eq. (1), is the sum of exponentially decaying harmonic functions with associated natural frequency f_{n_i} and of overdamped exponentially decaying functions. It can be found that η_i modal damping ratios linearly vary with respect to $\omega_{n_i} = 2\cdot\pi\cdot f_{n_i}$ modal natural frequencies [2]:

$$\eta_i = \min\left(\frac{\omega_{n_i}\cdot\beta}{2\cdot E_0}, 1\right), \tag{4}$$

so that the viscous β coefficient should also satisfy Eq. (4):

$$\beta = \frac{2\cdot E_0\cdot\eta_i}{\omega_{n_i}}. \tag{5}$$

Combining Eqs. (3,4):

$$\eta_i = \min(1.5\cdot\tau_c\cdot\omega_{n_i}, 1). \tag{6}$$

This result is typically not consistent with respect to the behavior of structures made of most known viscoelastic materials. As a matter of example, if High Density Polyethylene (HDPE) is considered, $E_0 = 1.08\cdot10^9$ Pa and $\tau_c \approx 100$ s result, and from Eq. (6), overdamped free vibrations ($\eta_i = 1$) analytically result if $f_{n_i} > (3\cdot\pi\cdot\tau_c)^{-1} \simeq 0.001$ Hz holds. In our laboratory facility experimental forced vibration input-output measurements were made on a uniform HDPE homogeneous beam, clamped-free boundary conditions, whose related data are reported in Table 1. Test FRF data were locally fitted by means of the circle fitting technique [20], and $\eta_i \in [0.01, 0.04]$ modal damping ratio values were identified as being almost constant in the $f_{n_i} \in [0, 7k]$ Hz wide frequency range, such result being not consistent with the values deriving from the creep time relaxation experimental estimate (Eq. (6)).

By modeling the HDPE material by means of a fractional Kelvin model:

$$\sigma(t) = E_0\cdot\left(\varepsilon(t) + \frac{\beta}{E_0}\cdot\frac{\partial^{\alpha}}{\partial t^{\alpha}}\varepsilon(t)\right); \quad 0 < \alpha < 1, \tag{7}$$

the creep relaxation $\varepsilon(t)$ response does not coincide with an exponential function anymore (Appendix A, Eq. A.1) and also the free response of a uniform, homogenous beam specimen is not the sum of underdamped and overdamped exponentially decaying harmonic functions anymore. The η_i modal damping ratios and ω_{n_i} circular frequencies of a uniform, homogenous beam specimen whose material follows Eq. (7) are not defined anymore when fractional derivative operators are adopted, but equivalent parameters may be defined as well by means of the procedure shown in Appendix A. Such procedure makes it possible to evaluate the equivalent damping ratio with respect to a given material model but an arbitrary beam structure, so $\eta = \eta(\omega)$ can be numerically estimated with respect to any ω value.

The equivalent damping ratio estimates $\eta(\omega)$, numerically obtained by means of the procedures described in Appendix A, by taking into account the different material models reported in Table 2 and the beam data in Table 1, are reported and compared with the experimental results in Figs. 1–2. In all of the example cases reported in Table 2 the material model data are consistent with the same HDPE material assumption: $E_0 \simeq 1.08\cdot10^9$ Pa and $\tau_c \simeq 100$ s.

Fig. 1 shows $\eta_i = \eta_i(f_{n_i} = \omega_{n_i}/2\pi)$ experimental and numerical results found with respect to (A-C) cases. The equivalent damping value estimates significantly increase with respect to frequency in the (A), (B) example cases (red and blue curves) related to a SLS model, and mostly overdamped free vibrations ($\eta_i = 100\%$) result. It appears that these numerical results are not consistent with respect to the experimental evidence (black curve). Even in the (C) example case (SLS model, $N = 2$, green curve), the consistency with the experimental results is only obtained in a limited frequency range (Fig. 1b). Fig. 2 shows $\eta_i = \eta_i(f_{n_i})$ experimental and numerical results found with respect to (D-H) cases.

In (D-G) cases, η_i monotonically increase with respect to ω_{n_i}, and the higher the fractional derivative order the higher the η_i. value results. H case appears to better fit experimental data results (Fig. 2b), since $\eta_i = \eta_i(\omega_{n_i})$ is not strictly increasing with ω_{n_i} circular frequency. It was found that structures made of a material following the SLS model, any N order, always exhibit high damping or overdamped behavior in the low and high frequency range, while a low N order, fractional SLS model can effectively be used to fit experimental measurements in a wide frequency

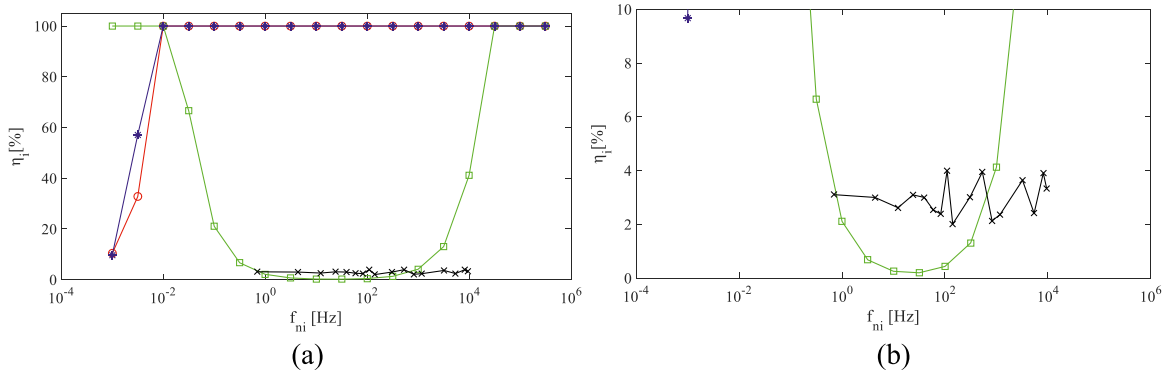

Fig. 1. (a) Damping ratio versus natural frequency: HDPE experimental results (black), (A) (red), (B) (blue) and (C) (green) example cases; (b) detail of (a).

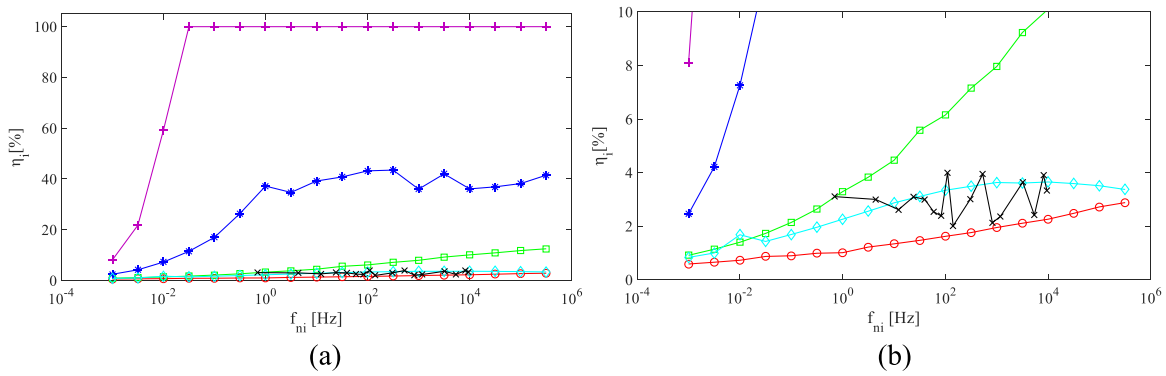

Fig. 2. (a) Damping ratio versus natural frequency: HDPE experimental results (black), (D) (purple), (E) (blue), (F) (green), (G) (red) and (H) (cyan) example cases; (b) detail of (a).

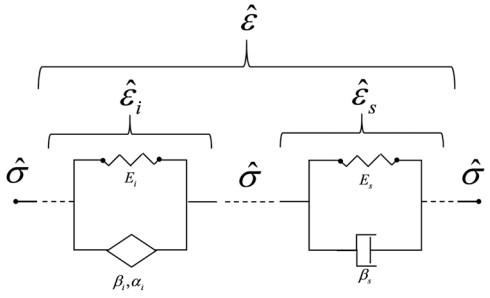

Fig. 3. Extended SLS model.

range.

3. Extended SLS material model identification from dynamical test measurements

The extended SLS material model taken into account in in this work results from a series arrangement of N_F fractional Kelvin and N_H hysteretic Kelvin elements (Fig. 3), so that Eq. (8) holds:

$$\hat{\varepsilon}=\sum_{i=1}^{N_F}\hat{\varepsilon}_i+\sum_{s=1}^{N_H}\hat{\varepsilon}_s \;;\; \hat{\varepsilon}_i=\frac{\hat{\sigma}}{E_i+(j\cdot\omega)^{\alpha_i}\cdot\beta_i},\; \hat{\varepsilon}_s=\frac{\hat{\sigma}}{E_s+j\cdot\omega\cdot\beta_s}$$
$$\frac{\hat{\varepsilon}}{\hat{\sigma}}=\frac{1}{E(j\cdot\omega)}=\Theta(j\cdot\omega)=\sum_{i=1}^{N_F}\frac{1}{E_i+(j\cdot\omega)^{\alpha_i}\cdot\beta_i}+\sum_{s=1}^{N_H}\frac{1}{E_s+j\cdot\omega\cdot\beta_s}=\left(\frac{\hat{\varepsilon}}{\hat{\sigma}}\right)_F+\left(\frac{\hat{\varepsilon}}{\hat{\sigma}}\right)_H \quad (8)$$

where $N=N_F+N_H$ is the extended SLS model order. Real valued positive elastic and dissipative parameters ($E_i, \beta_i, i=1...N_F$) and non-integer differential operators ($0<\alpha_i\le 1$) are assumed in the fractional Kelvin elements, and complex valued elastic and dissipative parameters (E_s, β_s, $s=1...N_H$) are assumed in the hysteretic Kelvin elements. Standard Kelvin elements can be modeled with fractional, $\alpha_i=1$, Kelvin elements.

The fractional and hysteretic contributions can be referred to as

$$\Theta(j\cdot\omega)=(E(j\cdot\omega))^{-1}=\left(\frac{\hat{\varepsilon}}{\hat{\sigma}}\right)_F+\left(\frac{\hat{\varepsilon}}{\hat{\sigma}}\right)_H=\Theta_F(j\cdot\omega)+\Theta_H(j\cdot\omega), \quad (9)$$

where $\Theta(j\cdot\omega_k), \omega_k\in[\omega_1...\omega_{N_x}]$ N_X complex data can be estimated from $\hat{\varepsilon}/\hat{\sigma}$ DMA test measurements, as it was previously outlined in the introduction.

The hysteretic Θ_H contribution is non-physical as it was previously indicated in the introduction.

The model identification problem can be stated as follows: find model parameters $E_i, \beta_i, \alpha_i, i=1...N_F, E_s, \beta_s, s=1...N_H$ best fitting the following N_X nonlinear equations in the unknown model parameters:

$$\Theta_k=\Theta(j\cdot\omega_k)=\Theta_F(j\cdot\omega_k)+\Theta_H(j\cdot\omega_k)$$
$$=\sum_{i=1}^{N_F}\frac{1}{E_i+(j\cdot\omega_k)^{\alpha_i}\cdot\beta_i}+\sum_{s=1}^{N_H}\frac{1}{E_s+j\cdot\omega_k\cdot\beta_s},\quad k=1...N_X. \quad (10)$$

The Θ_F contribution can be expressed as the ratio of two polynomial functions of the $j\cdot\omega$ complex variable, if standard Kelvin elements are considered ($\alpha_i=1,\ \forall i$), and same result applies with respect to the Θ_H contribution. Some algebraic techniques, based on the Levy's approach, are known from literature for the identification of the unknown parameters of the $\Theta_F(j\cdot\omega)$ in partial fraction form from experimental $\Theta(j\cdot\omega_k)$ test measurements [20], and this approach was applied in the past by these authors for the identification of the parameters of a SLS model [4]. The difference between measured and model estimated $\Theta_F(j\cdot\omega_k)$ values at any measured circular frequency ω_k value can be modelled by means of a residual polynomial in the $j\cdot\omega$ complex variable, whose optimal order can result from a least square best fit approach. It should be outlined that this approach, while meaningful from a mathematical fit standpoint is not coherent with respect to the extended SLS material model considered in this work.

A technique able to identify the optimal $\Theta_F(j\cdot\omega)$ model fitting $\Theta(j\cdot\omega_k), \forall k$ experimental data is shown. The model error vector $\mathbf{\Delta\Theta}$ obtained as the difference between experimental $\Theta(j\cdot\omega_k)$ data and $\Theta_F(j\cdot\omega_k)$ data values estimated from the identified model, $\forall k$, is then used to identify the $\Theta_H(j\cdot\omega)$ hysteretic model proposed. Two different identification techniques are thus proposed in the following sections to separately identify the $\Theta_F(j\cdot\omega)$ and $\Theta_H(j\cdot\omega)$ contributions.

3.1. Θ_F identification

3.1.1. Θ_F model equivalent formulation

The Θ_F model defined in Eq.8 leads to a highly nonlinear equation of the α_i, E_i, β_i model unknown parameters. An equivalent Θ_F formulation is obtained and proposed here in order to be compatible with the linear identification approach that will be described in Section 3.1.2.

Fractional derivative order is assumed for any Θ_F element:

$$\alpha_i=\frac{n_i}{D},\quad i=1,...,N_F,\quad 1\le n_i\le D \quad (11)$$

where $n_i, D\in\mathbb{N}$, and D value is assumed to be high enough to approxi-

mate α_i unknown value, $\forall i$. From Eqs. (8,11):

$$\Theta_F(j\cdot\omega)=\sum_{i=1}^{N_F}\frac{1}{E_i+(j\cdot\omega)^{\alpha_i}\cdot\beta_i}=\sum_{i=1}^{N_F}\frac{1/\beta_i}{(j\cdot\omega)^{\frac{n_i}{D}}+\frac{E_i}{\beta_i}}=\sum_{i=1}^{N_F}\frac{R_i}{q^{n_i}+\gamma_i},$$
$$q=(j\cdot\omega)^{\frac{1}{D}},\quad \gamma_i=\frac{E_i}{\beta_i},\quad R_i=\quad 1/\beta_i, \tag{12}$$

where $R_i,\ \gamma_i\in\Re^+$. Since:

$$q^{n_i}+\gamma_i=\prod_{s=1}^{n_i}(q-z_{i,s}),$$
$$z_{i,s}=(\gamma_i)^{\frac{1}{n_i}}\cdot e^{j\cdot\frac{\pi\cdot(1+2\cdot(s-1))}{n_i}},\ s=1,.,n_i,\ i=1,.,N_F;$$
$$|z_{i,s}|=(\gamma_i)^{\frac{1}{n_i}}=\left(\frac{E_i}{\beta_i}\right)^{\frac{1}{n_i}}, \tag{13}$$
$$\Delta\arg(z_i)=\ \arg(z_{i,s+1})-\arg(z_{i,s})=\frac{2\cdot\pi}{n_i},\ \forall s<n_i,\ i=1,.,N_F,$$

and:

$$\frac{R_i}{q^{n_i}+\gamma_i}=\sum_{s=1}^{n_i}\frac{r_{i,s}}{q-z_{i,s}},$$
$$r_{i,s}=\lim_{q\to z_{i,s}}\left[\frac{R_i}{q^{n_i}+\gamma_i}\cdot(q-z_{i,s})\right]=\frac{R_i}{\prod_{\substack{\ell=1\\ \ell\neq s}}^{n_i}(z_{i,s}-z_{i,\ell})}. \tag{14}$$

From Eq. (12):

$$\frac{q^{n_i}+\gamma_i}{q-z_{i,s}}=\prod_{\substack{\ell=1\\ \ell\neq s}}^{n_i}(q-z_{i,\ell}),\qquad q\neq z_{i,s}, \tag{15}$$

and from Eqs.14–15:

$$\lim_{q\to z_{i,s}}\left(\frac{q^{n_i}+\gamma_i}{q-z_{i,s}}\right)=\prod_{\substack{\ell=1\\ \ell\neq s}}^{n_i}(z_{i,s}-z_{i,\ell})=\frac{R_i}{r_{i,s}}. \tag{16}$$

Function $g(q)=q^n$ is defined, so that from Eqs. (12–16) the following results can be obtained, $\forall i,s$:

$$g(q=z_{i,s})=(z_{i,s})^{n_i}=-\gamma_i; \tag{17}$$

$$\frac{dg}{dq}(q=z_{i,s})=n_i\cdot(z_{i,s})^{n_i-1}=n_i\cdot\frac{(z_{i,s})^{n_i}}{z_{i,s}}=-\frac{n_i\cdot\gamma_i}{z_{i,s}}; \tag{18a}$$

$$\frac{dg}{dq}(q=z_{i,s})=\lim_{q\to z_{i,s}}\frac{g(q)-g(z_{i,s})}{q-z_{i,s}}=\lim_{q\to z_{i,s}^{\prime}}\left(\frac{q^{n_i}+\gamma_i}{q-z_{i,s}}\right)=\frac{R_i}{r_{i,s}}. \tag{18b}$$

From Eq. (18a-b):

$$r_{i,s}=-\frac{R_i\cdot z_{i,s}}{n_i\cdot\gamma_i}=-\frac{z_{i,s}}{n_i\cdot E_i},$$
$$|r_{i,s}|=\frac{1}{n_i\cdot E_i}\cdot\left(\frac{E_i}{\beta_i}\right)^{\frac{1}{n_i}}=\frac{1}{n_i\cdot\left(E_i^{n_i-1}\cdot\beta_i\right)^{\frac{1}{n_i}}}, \tag{19}$$
$$\arg(r_{i,s})=\arg(z_{i,s})+\pi,\ \ \forall s<n_i,$$
$$\Delta\arg(r_i)=\ \arg(r_{i,s+1})-\arg(r_{i,s})=\frac{2\cdot\pi}{n_i},\ \ \forall s<n_i.$$

From Eqs. (12,13) Θ_F can be expressed in partial fraction form:

$$\Theta_F=\sum_{i=1}^{N_F}\left(\sum_{s=1}^{n_i}\frac{r_{i,s}}{q-z_{i,s}}\right)=\frac{\sum_{\ell=0}^{m-1}q^{\ell}\cdot a_{\ell}}{q^m+\sum_{\ell=0}^{m-1}q^{\ell}\cdot b_{\ell}.}=\frac{q^{m-1}\cdot a_{m-1}+\ldots+a_0}{q^m+q^{m-1}\cdot b_{m-1}+\ldots+b_0}=\sum_{\ell=1}^{m}\frac{r_i}{q-z_i},$$
$$m=\sum_{i=1}^{N_F}n_i;\ \mathbf{r}=[r_1,\ldots,r_m]=\left[r_{1,1},\ldots,r_{1,n_1},\ldots,r_{N_F,n_{N_F}}\right],$$
$$\mathbf{z}=[z_1,\ldots,z_m]=\left[z_{1,1},\ldots,z_{1,n_1},\ldots,z_{N_F,n_{N_F}}\right]. \tag{20}$$

Since $n_i\in\mathbb{N}$ and $R_i,\ \gamma_i\in\Re^+$, it follows that $a_{\ell},b_{\ell}\in\Re^+,\ \forall\ell$.

3.1.2. Θ_F non-parametric model identification technique

It is assumed that Θ_k measurement test estimates at circular frequency $\omega_k,\quad k=1,\ldots,N_X$, are available, and:

$$q_k=(j\cdot\omega_k)^{1/D}. \tag{21}$$

The optimal Θ_F fractional SLS material model (Eq. (20)) fitting measured values can be found by arbitrarily choosing m and by identifying the a_{ℓ} and b_{ℓ} real unknowns ($\ell=0\ldots m-1$), best fitting the experimentally estimated values:

$$\Theta_k=\frac{\sum_{\ell=0}^{m-1}(q_k)^{\ell}\cdot a_{\ell}}{(q_k)^m+\sum_{\ell=0}^{m-1}(q_k)^{\ell}\cdot b_{\ell}},\qquad k=1\ldots N_X. \tag{22}$$

A system of N_X linear equations in (a_{ℓ}, b_{ℓ}), $2\cdot m$ unknowns, results:

$$\sum_{\ell=0}^{m-1}(q_k)^{\ell}\cdot a_{\ell}-\sum_{\ell=0}^{m-1}\Theta_k\cdot(q_k)^{\ell}\cdot b_{\ell}=\Theta_k\cdot(q_k)^m. \tag{23}$$

If a large set of test measurements, e.g., $N_X\gg\ 2\cdot m$, and high m value is taken into account, the numerical solution of Eq. (23) is expected to be ill-conditioned, requiring the pseudo inversion of a high order Vandermonde-like coefficient matrix. To increase the system matrix condition and improve the computational accuracy of the solution, a normalized variable $u=(\omega/\omega_{N_X})^{1/D}\in[0,1]$ is introduced:

$$u_k=\frac{|q_k|}{|q_{N_X}|},\qquad u_k\in[0,1],$$
$$q_k=(j\cdot\omega_k)^{\frac{1}{D}}=|q_k|\cdot e^{j\cdot\phi}=u_k\cdot|q_{N_X}|\cdot e^{j\cdot\phi}\quad\cdot \tag{24}$$
$$(q_k)^{\ell}=(u_k)^{\ell}\cdot|q_{N_X}|^{\ell}\cdot e^{j\cdot\phi\cdot\ell};\quad \phi=\frac{\pi}{2\cdot D}$$

From Eq. (23,24):

$$\sum_{\ell=0}^{m-1}(u_k)^{\ell}\cdot|q_{N_X}|^{\ell}\cdot e^{j\cdot\phi\cdot\ell}a_{\ell}-\sum_{\ell=0}^{m-1}\Theta_k\cdot(u_k)^{\ell}\cdot|q_{N_X}|^{\ell}\cdot e^{j\cdot\phi\cdot\ell}\cdot b_{\ell}=\Theta_k\cdot(u_k)^m\cdot|q_{N_X}|^m\cdot e^{j\cdot\phi\cdot m}$$
$$\sum_{\ell=0}^{m-1}(u_k)^{\ell}\cdot e^{j\cdot\phi\cdot(\ell-m)}\cdot\tilde{a}_{\ell}-\sum_{\ell=0}^{m-1}\Theta_k\cdot(u_k)^{\ell}\cdot e^{j\cdot\phi\cdot(\ell-m)}\cdot\tilde{b}_{\ell}=\Theta_k\cdot(u_k)^m,\qquad k=1\ldots N_X\ ,$$
$$\tilde{a}_{\ell}=|q_{N_X}|^{\ell-m}\cdot a_{\ell},\quad \tilde{b}_{\ell}=|q_{N_X}|^{\ell-m}\cdot b_{\ell}\ . \tag{25}$$

where the following linear transformation was used in Eq. (25) for computational purposes:

$$\mathbf{a}=[\,a_0\quad\ldots\quad a_{\ell}\quad\ldots\quad a_{m-1}\,]^T,\mathbf{b}=[\,b_0\quad\ldots\quad b_{\ell}\quad\ldots\quad b_{m-1}\,]^T;$$
$$\mathbf{q}=\left[\,(\omega_{N_X})^{-m/D}\quad\ldots\quad(\omega_{N_X})^{(\ell-m)/D}\quad\ldots\quad(\omega_{N_X})^{-1/D}\,\right]^T\in\Re^m; \tag{26}$$
$$\tilde{\mathbf{a}}=diag(\mathbf{q})\cdot\mathbf{a},\quad \tilde{\mathbf{b}}=diag(\mathbf{q})\cdot\mathbf{b}\ .$$

A linear system of $2\cdot N_X$ real equations in the $\tilde{\mathbf{a}}$, $\tilde{\mathbf{b}}$ real unknowns results:

Table 3
(I) Test case model identification results.

Reference model				Identified model				$E/E_0(j\cdot\omega)$ quadratic error fit
	α_i	E_i [Pa]	β_i [Pa•s$^{\alpha}$]		α_i	E_i [Pa]	β_i [Pa•s$^{\alpha}$]	
N_F =2	0.1 0.2	9.08•10^9 5.25.10^9	6.42•10^8 4.95.10^8	N_F =2	0.1 0.2	9.08•10^9 5.25.10^9	6.42•10^8 4.95.10^8	2.24 10^{-6}

Table 4
(L) Test case model identification results.

Reference model				Identified model				$E/E_0(j\cdot\omega)$ quadratic error fit
	α_i	E_i [Pa]	β_i [Pa•s$^{\alpha}$]		α_i	E_i [Pa]	β_i [Pa•s$^{\alpha}$]	
N_F =1	0.25	1.08•10^9	3.85•10^7	N_F =1	0.2	1.08•10^9	3.86•10^8	
N_H =1	1	1.58•10^{11}+ +j•6.03.10^9	7.50•10^7+ +j•1.11.10^7	N_H =1	1	1.58•10^{10} +j•1.70.10^9	7.49•10^7 +j•1.16.10^7	2.93•10^{-6}

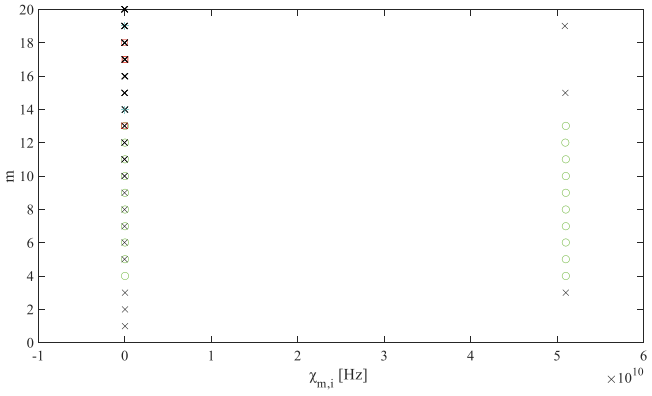

Fig. 4. (I) test case Θ_F stability plot, identified stable and unstable solutions marked according to Table. B.1.

$$\begin{bmatrix} \mathrm{Re}(\mathbf{A}) & -\mathrm{Re}(\mathbf{B}) \\ \mathrm{Im}(\mathbf{A}) & -\mathrm{Im}(\mathbf{B}) \end{bmatrix} \cdot \begin{bmatrix} \tilde{\mathbf{a}} \\ \tilde{\mathbf{b}} \end{bmatrix} = \begin{bmatrix} \mathrm{Re}(\mathbf{O}) \\ \mathrm{Im}(\mathbf{O}) \end{bmatrix};$$

$$\mathbf{A} = \begin{bmatrix} e^{-j\cdot\phi\cdot m} & u_1\cdot e^{j\cdot\phi\cdot(1-m)} & \dots & (u_1)^{m-1}\cdot e^{-j\cdot\phi} \\ \dots & \dots & \dots & \dots \\ e^{-j\cdot\phi\cdot m} & u_{N_X}\cdot e^{j\cdot\phi\cdot(1-m)} & \dots & (u_{N_X})^{m-1}\cdot e^{-j\cdot\phi} \end{bmatrix},$$

$$\mathbf{B} = \begin{bmatrix} \Theta_1\cdot e^{-j\cdot\phi\cdot m} & \Theta_1\cdot u_1\cdot e^{j\cdot\phi\cdot(1-m)} & \dots & \Theta_1\cdot(u_1)^{m-1}\cdot e^{-j\cdot\phi} \\ \dots & \dots & \dots & \dots \\ \Theta_{N_X}\cdot e^{-j\cdot\phi\cdot m} & \Theta_{N_X}\cdot u_{N_X}\cdot e^{j\cdot\phi\cdot(1-m)} & \dots & \Theta_{N_X}\cdot(u_{N_X})^{m-1}\cdot e^{-j\cdot\phi} \end{bmatrix}, \quad (27)$$

$$\mathbf{O} = [\,\Theta_1\cdot(u_1)^m \quad \dots \quad \Theta_{N_X}\cdot(u_{N_X})^m\,]^T.$$

The $\tilde{\mathbf{a}}, \tilde{\mathbf{b}}$ unknown real coefficients can be obtained by least squares solving Eq. (27) by means of a Singular Value Decomposition (SVD) based technique, so that from Eq. (26) $\mathbf{a} = (diag(\mathbf{q}))^{-1}\cdot\tilde{\mathbf{a}}$, $\mathbf{b} = (diag(\mathbf{q}))^{-1}\cdot\tilde{\mathbf{b}}$ results as well.

It should be outlined that since the solution can be found with respect to any m assumed value, $\mathbf{a} = (\mathbf{a})_m$, $\mathbf{b} = (\mathbf{b})_m$. An iterative approach, based on the evaluation of the stability of $(\mathbf{a})_m$, $(\mathbf{b})_m$ solution is proposed herein [15]. For any $m = 1,2,3,\dots,m_{\max}$, the system $(\mathbf{z})_m$ poles can also be evaluated from $(\mathbf{b})_m$ as the m zeros of the following polynomial function:

$$z^m + z^{m-1}\cdot b_{m-1} + \dots + b_0 = 0. \quad (28)$$

System $(\mathbf{r})_m$ residues can be evaluated from $(\mathbf{z})_m, (\mathbf{a})_m$ as follows:

$$r_\ell = \lim_{q\to z_\ell}\left[\sum_{i=1}^{m}\frac{r_i}{q-z_i}\cdot(q-z_\ell)\right] = \frac{\sum_{i=0}^{m-1} a_i\cdot(z_\ell)^i}{\prod_{\substack{i=1\\ i\neq\ell}}^{m}(z_\ell - z_i)}. \quad (29)$$

The $\tilde{\mathbf{z}}_i = [\tilde{z}_{i,1},\dots,\tilde{z}_{i,n_i}]^T \in (\mathbf{z})_m$, $\tilde{\mathbf{r}}_i = [\tilde{r}_{i,1},\dots,\tilde{r}_{i,n_i}]^T \in (\mathbf{r})_m$ $i = 1\dots(N_F)_m$ subsets belonging to i-th fractional Kelvin element, $\alpha_i = n_i/D$ fractional order, can be found by means of the procedure reported in Appendix B. The $\tilde{\mathbf{z}}_i$, $\tilde{\mathbf{r}}_i$ elements exhibit constant modulus and constant $\Delta\arg()$ relative phase (Eqs. (13,19)):

$$\begin{aligned} &n_i = size\left(\tilde{\mathbf{z}}_i\right) = size\left(\tilde{\mathbf{r}}_i\right), \\ &\Delta\arg\left(\tilde{\mathbf{z}}_i\right) \simeq \frac{2\pi}{n_i}, \quad \Delta\arg\left(\tilde{\mathbf{r}}_i\right) \simeq \frac{2\pi}{n_i}, \\ &\left|\tilde{z}_{i,s}\right| \simeq const, \quad \left|\tilde{r}_{i,s}\right| \simeq const, \quad \arg\left(\tilde{z}_{i,1}\right) \simeq \frac{\pi}{n_i}; \quad \forall s, \\ &\arg\left(\tilde{r}_{i,s}\right) \simeq \arg\left(\tilde{z}_{i,s}\right) + \pi; \quad \forall s. \end{aligned} \quad (30)$$

The parameters associated to i-th fractional Kelvin element can be identified from Eqs. (13,19):

$$E_i = \frac{\sum_{s=1}^{n_i}\left|\tilde{z}_{i,s}\right|}{n_i\cdot\sum_{s=1}^{n_i}\left|\tilde{r}_{i,s}\right|}, \qquad \beta_i = \frac{1}{R_i} = E_i\cdot\left(\frac{n_i}{\sum_{s=1}^{n_i}\left|\tilde{z}_{i,s}\right|}\right)^{n_i}, \qquad \alpha_i = \frac{n_i}{D}, \qquad \gamma_i = \frac{E_i}{\beta_i}. \quad (31)$$

The identified fractional elements being stable with respect to different m values can be selected as the constituents of the extended SLS model, while the other identified fractional elements, only resulting from the computational evaluation can be discarded. The stability approach, commonly used in most modal analysis procedures [20], is adopted, making it possible to automatically or manually select stable solutions taking into account user defined tolerance values.

The $\Theta_F(j\cdot\omega)$ model $\{\{E_1, \beta_1, \alpha_1, \gamma_1, R_1\}, \dots, \{E_{(N_F)_m}, \beta_{(N_F)_m}, \alpha_{(N_F)_m}, \gamma_{(N_F)_m}, R_{(N_F)_m}\}\}_m$ is identified, and is compared to $\{\{E_1, \beta_1, \alpha_1, \gamma_1, R_1\}, \dots, \{E_{(N_F)_{m-1}}, \beta_{(N_F)_{m-1}}, \alpha_{(N_F)_{m-1}}, \gamma_{(N_F)_{m-1}}, R_{(N_F)_{m-1}}\}\}_{m-1}$ by evaluating the stability with respect to α_i, γ_i, R_i. The stability properties of $\{E_i, \beta_i, \alpha_i, \gamma_i, R_i\}_m$ i-th solution associated with the m-value identification step can be associated to a marker according to the Table B1 specifications and plotted in the stability graph with respect to $\chi_{m,i} = |E_i/\beta_i|^{1/\alpha_i}$ frequency abscissa value and m ordinate value. The stability procedure is detailed in Appendix B.

To show the effectiveness of the stability approach, $N_X = 1000$ simulated measurements are numerically evaluated from (I) (Table 3) and (L) (Table 4) test cases, in the $\omega \in [10^{-1}, 10^3]$ Hz frequency range. A

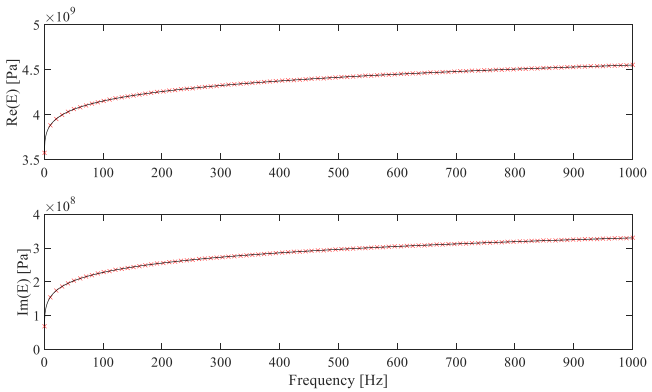

Fig. 5. (I) test case: $E(j{\cdot}\omega)$ simulated measurements (black) and identified model fit (red).

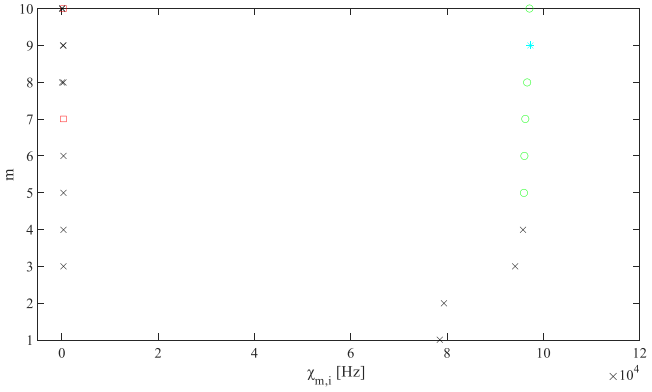

Fig. 6. (L) test case Θ_F stability plot, identified stable and unstable solutions marked according to Table. B.1.

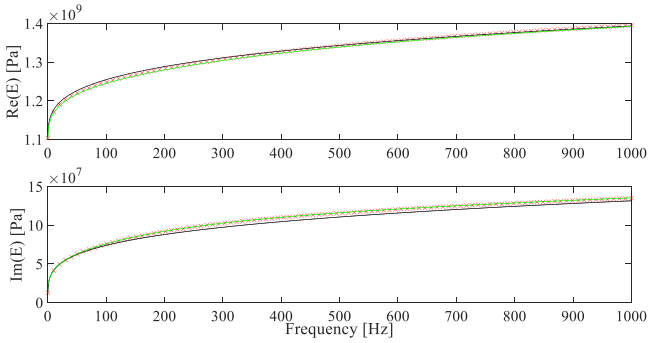

Fig. 7. (L) test case: $E(j{\cdot}\omega)$ simulated measurements (red), (N_F=1) fractional SLS model fit (black), (N_F=1, N_H=1) extended SLS model fit (green).

stability diagram is shown in Fig. 4 reporting model solutions obtained with respect to the (I) test case simulated measurements, identification parameters are $D = 10$, $m_{\max} = 20$. Two fractional SLS element stable solutions are found, corresponding to the $N_F = 2$ identified fractional SLS model reported in Table 3, showing an excellent agreement with reference values. Fig. 5 shows $E(j{\cdot}\omega)$ plot from the $\Theta(j{\cdot}\omega_k)$ simulated measurements and the model identified $\Theta_F(j{\cdot}\omega)$ estimate, where the error difference between measured and the model identified estimate is negligible.

Fig. 6 reports the stability diagram obtained from model identification obtained with respect to (L) test case simulated measurements, identification parameters are $D = 4$, $m_{\max} = 10$. A single fractional, SLS element stable solution is found starting from $m = 4$, corresponding to

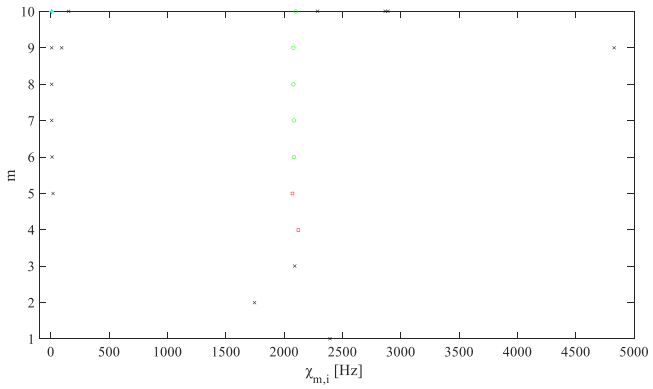

Fig. 8. (L) test case Θ_H stability plot, identified stable and unstable solutions marked according to Table. B.1.

the $N_F = 1$ identified fractional SLS model reported in Table 4, showing a good agreement with reference values. Fig. 7 shows the simulated measurements plot and the $\Theta_F(j{\cdot}\omega)$ model identified plot, the error difference between the two curves being mainly due to the lacking contribution of the still unidentified hysteretic model component.

It should be outlined that a Θ_F physical model, being consistent with thermodynamic isothermal assumptions, must satisfy the following conditions [6]:

$$\Re(\Theta(j{\cdot}\omega))^{-1} \geq 0, \quad \Im(\Theta(j{\cdot}\omega))^{-1} \geq 0, \quad 0 < \omega < \infty. \tag{32}$$

Some more restrictions on the fractional SLS $\{E_i,\ \beta_i,\ \alpha_i, \gamma_i, R_i\}_m$ parameters should apply from Eq. (32), and their evaluation will be considered in our future research. It should be outlined that all of the identification results shown in this paper respect the Eq. (32) condition, since test data consisting in $E(j{\cdot}\omega_k)$ material measured estimates appears to respect Eq. (32) condition as well.

3.2. Θ_H identification

3.2.1. Θ_H model formulation

From Eq. (8-9) the hysteretic Kelvin elements contribution is:

$$\Theta_H(j{\cdot}\omega) = \sum_{i=1}^{N_H} \frac{1/\beta_i}{j{\cdot}\omega + \frac{E_i}{\beta_i}} = \sum_{i=1}^{N_H} \frac{R_i}{j{\cdot}\omega - z_i}; \qquad z_i = -\frac{E_i}{\beta_i}, \quad R_i = 1/\beta_i \tag{33}$$

where $E_i, \beta_i, R_i, z_i \in \mathbb{C}$. From Eq. (33), $\Theta_H(j{\cdot}\omega)$ can also be expressed as the ratio of two polynomials:

$$\Theta_H = \frac{(j{\cdot}\omega)^{N_H-1}{\cdot}c_{N_H-1} + \ldots + c_0}{(j{\cdot}\omega)^{N_H} + (j{\cdot}\omega)^{N_H-1}{\cdot}d_{N_H-1} + \ldots + d_0} = \frac{\sum_{i=0}^{N_H-1} (j{\cdot}\omega)^i{\cdot}c_i}{(j{\cdot}\omega)^{N_H} + \sum_{i=0}^{N_H-1} (j{\cdot}\omega)^i{\cdot}d_i}, \tag{34}$$

and since $R_i,\ z_i \in \mathbb{C}$, it follows that $a_i,\ b_i \in \mathbb{C}\ ,\ \forall i$.

3.2.2. Θ_H non-parametric model identification technique

$\Theta_H(j{\cdot}\omega)$ can be estimated from Eq.10:

$$\Delta\Theta_k = \Theta_k - \Theta_F(j{\cdot}\omega_k) = \Theta_H(j{\cdot}\omega_k) = \frac{\sum_{i=0}^{m-1} (j{\cdot}\omega_k)^i{\cdot}a_i}{(j{\cdot}\omega_k)^m + \sum_{i=0}^{m-1} (j{\cdot}\omega_k)^i{\cdot}b_i}, \quad k = 1\ldots N_X. \tag{35}$$

The optimal Θ_H hysteretic SLS material model fitting $\Delta\Theta_k$ values can

Table 5
Numerical fractional SLS model identification results.

Case	Reference model				Identified model				$E/E_0(j\cdot\omega)$ quadratic error fit
		α_i	E_i [Pa]	β_i [Pa•s$^{\alpha}$]	N_F	α_i	E_i [Pa]	β_i [Pa•s$^{\alpha}$]	
(M)	$N_F=2$	0.3	$9.13\bullet10^{8}$	$3.37\bullet10^{9}$	$N_F=2$	0.3	$9.13\bullet10^{8}$	$3.382\bullet10^{9}$	$3.6\bullet10^{-7}$
		0.2	$6.03\bullet10^{8}$	$1.52\bullet10^{8}$		0.2	$6.03\bullet10^{8}$	$1.5203\bullet10^{8}$	
(N)	$N_F=3$	0.5	$9.21\bullet10^{10}$	$1.04\bullet10^{9}$	$N_F=3$	0.5	$9.21\bullet10^{10}$	$8.02\bullet10^{9}$	$2.15\bullet10^{-4}$
		0.75	$1.01\bullet10^{11}$	$3.11\bullet10^{11}$		0.75	$1.01\bullet10^{11}$	$3.11\bullet10^{11}$	
		0.25	$9.41\bullet10^{8}$	$8.02\bullet10^{9}$		0.25	$9.41\bullet10^{8}$	$8.02\bullet10^{9}$	
(O) (no S/N)	$N_F=2$	0.25	$2.25\bullet10^{9}$	$4.21\bullet10^{9}$	$N_F=2$	0.25	$2.25\bullet10^{9}$	$4.20\bullet10^{9}$	$2.23\bullet10^{-6}$
		0.5	$9.15\bullet10^{8}$	$9.31\bullet10^{6}$		0.5	$9.15\bullet10^{8}$	$9.32\bullet10^{6}$	
(O) (90 dB S/N)	$N_F=2$	0.25	$2.25\bullet10^{9}$	$4.21\bullet10^{9}$	$N_F=2$	0.25	$2.10\bullet10^{9}$	$3.78\bullet10^{9}$	$1.05\bullet10^{-2}$
		0.5	$9.15\bullet10^{8}$	$9.31\bullet10^{6}$		0.5	$9.35\bullet10^{8}$	$1.03\bullet10^{7}$	

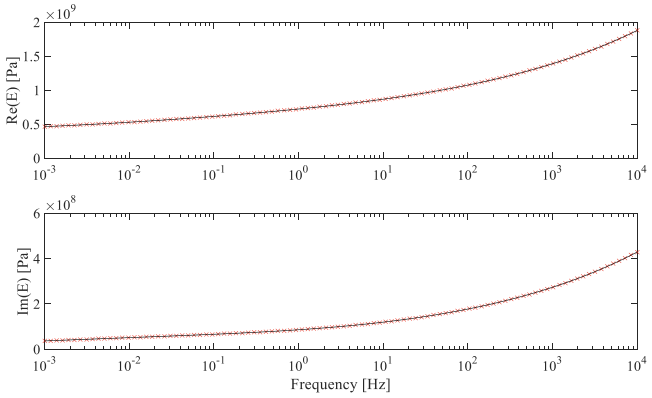

Fig. 9. (M) example case: $E(j\cdot\omega)$ model (red), identified model fit (black).

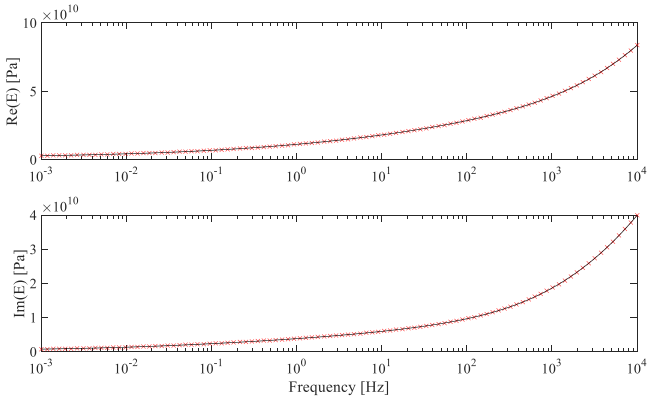

Fig. 10. (N) example case: $E(j\cdot\omega)$ model (red), identified model fit (black).

be found by arbitrarily choosing m and by identifying the a_i, b_i $i = 0\ldots m-1$, complex unknowns, best fitting the $\Delta\Theta_k$values. A complex system of N_X linear complex equations in the $2\cdot m$, a_i, b_i, $i = 0\ldots m-1$, complex unknowns results:

$$\sum_{i=0}^{m-1}(j\cdot\omega_k)^i\cdot a_i - \sum_{i=0}^{m-1}\Delta\Theta_k\cdot(j\cdot\omega_k)^i\cdot b_i = \Delta\Theta_k\cdot(j\cdot\omega_k)^m; \tag{36}$$

$k = 1\ldots N_X$.

To increase the system matrix condition and improve the computational accuracy of the solution, a normalized variable $u = (\omega/\omega_{N_X}) \in [0,1]$ is introduced. From Eq. (36):

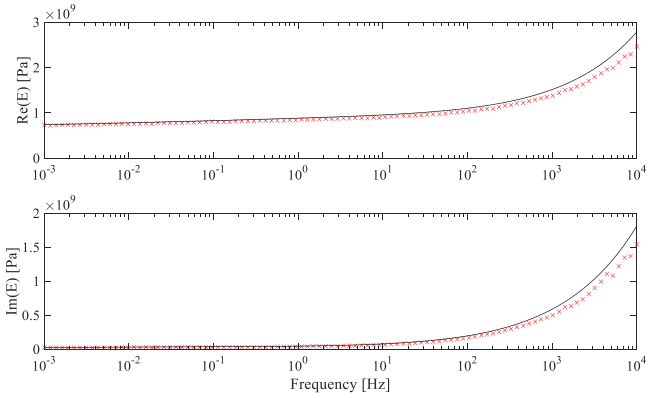

Fig. 11. (O) example case: $E(j\cdot\omega)$ model with 90 dB S/N added noise (red), identified curve fit (black).

Table 6
specimen experimental data.

Beam specimen	Material	Length [m]	Section Area [m^2]	E_0 [Pa]	Density [kg/m^3]
(BS1)	Loxeal instant 47 gel® (85 % volume ratio) and steel powder (10 μm mean grain size, 15 % volume ratio) mix	$1.75\bullet10^{-2}$	$9.02\bullet10^{-6}$	$1.70\bullet10^{9}$	$2.00\bullet10^{3}$
(BS2)	Loxeal 31–10® (60 % 31-component and 30 % 10-component volume fractions) and carbon fibers (length 60–300 μm, 10 % volume fraction) mix	$1.75\bullet10^{-2}$	$5.84\bullet10^{-6}$	$2.38\bullet10^{9}$	$1.11\bullet10^{3}$

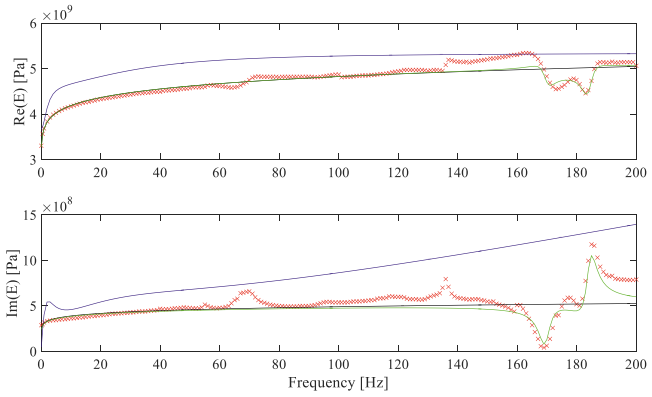

Fig. 12. (BS1) test case: $E(j{\cdot}\omega)$ measurement data (red), SLS model fit (blue), fractional SLS model fit (black), extended SLS model fit (green).

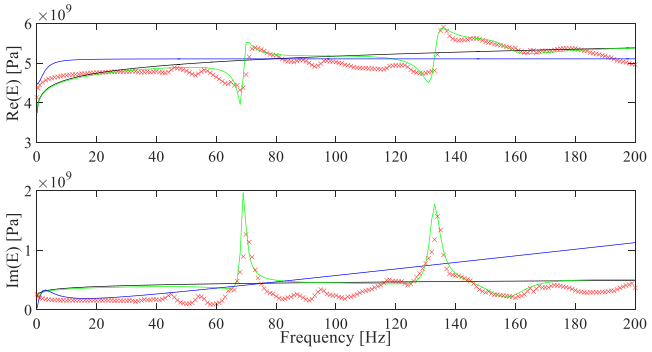

Fig. 13. (BS2) test case: $E(j{\cdot}\omega)$ measurement data (red), SLS model fit (blue), fractional SLS model fit (black), extended SLS model fit (green).

$$\sum_{i=0}^{m-1}(u_k)^i{\cdot}(j{\cdot}\omega_{N_X})^i{\cdot}a_i-\sum_{i=0}^{m-1}\Delta\Theta_k{\cdot}(u_k)^i{\cdot}(j{\cdot}\omega_{N_X})^i{\cdot}b_i=\Delta\Theta_k{\cdot}(u_k)^m{\cdot}(j{\cdot}\omega_{N_X})^m$$
$$\sum_{i=0}^{m-1}(u_k)^i{\cdot}\tilde{a}_i-\sum_{i=0}^{m-1}\Delta\Theta_k{\cdot}(u_k)^i{\cdot}\tilde{b}_i=\Delta\Theta_k{\cdot}(u_k)^m,$$
$$\tilde{a}_i=(j{\cdot}\omega_{N_X})^{i-m}{\cdot}a_i,\quad \tilde{b}_i=(j{\cdot}\omega_{N_X})^{i-m}{\cdot}b_i\,;\qquad k=1\ldots N_X, \tag{37}$$

where the following linear transformation was used in Eq. (37) for computational purposes:

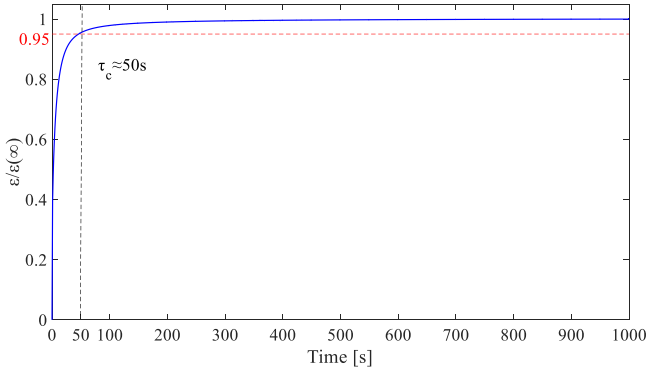

Fig. A1. τ_c evaluation for (A1) example case.

Table A1
(A1) example case model parameters.

	α_i	E_i [Pa]	β_i [Pa•s^a]
N_F= 3	0.3	$5{\bullet}10^{10}$	$1{\bullet}10^{8}$
	0.8	$1{\bullet}10^{10}$	$5{\bullet}10^{10}$
	0.5	$7{\bullet}10^{10}$	$3{\bullet}10^{9}$

Table 7
Experimental test cases: extended SLS model identification results.

Case	Extended SLS model						$E/E_0(j{\cdot}\omega)$ quadratic error fit
		α_i	E_i [Pa]	β_i [Pa•s$^\alpha$]	E_0 [Pa]	τ_c [s]	
(BS1)	N_F =2	0.1	$1.73{\bullet}10^{9}$	$1.65{\bullet}10^{9}$	$1.73{\bullet}10^{9}$	$2.01{\bullet}10^{12}$	$6.84{\bullet}10^{-3}$
		0.2	$1.12{\bullet}10^{13}$	$2.78{\bullet}10^{12}$			
	N_H =2	1	$3.13{\bullet}10^{12}$-$j{\bullet}2.07{\bullet}10^{12}$	$1.82{\bullet}10^{9}$+$j{\bullet}2.69{\bullet}10^{9}$			
		1	$-3.56{\bullet}10^{12}$-$j{\bullet}2.66{\bullet}10^{11}$	$2.45{\bullet}10^{8}$-$j{\bullet}3.37{\bullet}10^{9}$			
(BS2)	N_F =2	0.2	$5.977{\bullet}10^{10}$	$2.672{\bullet}10^{10}$	$2.38{\bullet}10^{9}$	$1.69{\bullet}10^{10}$	$1.23{\bullet}10^{-2}$
		0.1	$2.484{\bullet}10^{9}$	$1.503{\bullet}10^{9}$			
	N_H =3	1	$-1.67{\bullet}10^{12}$-$j{\bullet}7.64{\bullet}10^{11}$	$6.84{\bullet}10^{8}$-$j{\bullet}1.74{\bullet}10^{9}$			
		1	$-1.31{\bullet}10^{12}$-$j{\bullet}1.06{\bullet}10^{11}$	$1.52{\bullet}10^{8}$+$j{\bullet}1.57{\bullet}10^{9}$			
		1	$1.07{\bullet}10^{12}$-$j{\bullet}2.39{\bullet}10^{11}$	$5.87{\bullet}10^{8}$+$j{\bullet}2.47{\bullet}10^{9}$			

Table 8
Experimental test cases: SLS model identification results.

Case	SLS model					$E/E_0(j{\cdot}\omega)$ quadratic error fit
		α_i	E_i [Pa]	β_i [Pa•s$^\alpha$]	E_0 [Pa]	τ_c [s]	
(BS1)	N =3	1	$5.41{\bullet}10^{9}$	$1.02{\bullet}10^{6}$	$3.67{\bullet}10^{9}$	$1.38{\bullet}10^{-1}$	$3.01{\bullet}10^{-2}$
		1	$3.42{\bullet}10^{10}$	$1.93{\bullet}10^{8}$			
		1	$1.71{\bullet}10^{10}$	$1.62{\bullet}10^{9}$			
(BS2)	N =2	1	$5.18{\bullet}10^{9}$	$8.92{\bullet}10^{5}$	$4.47{\bullet}10^{9}$	$6.40{\bullet}10^{-2}$	$1.31{\bullet}10^{-1}$
		1	3.57•1010	$2.48{\bullet}10^{9}$			

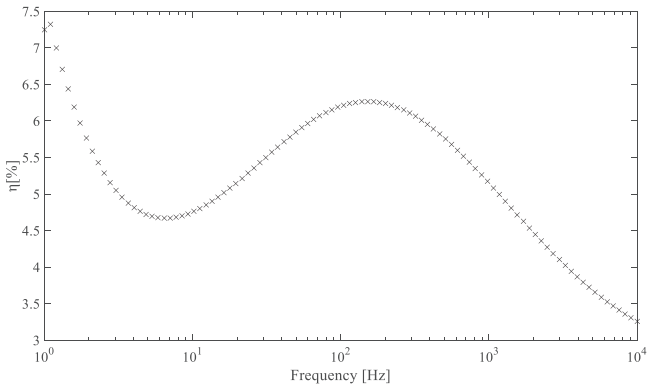

Fig. A2. Example case (A1):$\eta(\omega)$estimated values.

Table B1
Solution stability conditions.

Stability evaluation	Condition	Marker
Unstable	$\left\|\frac{(\gamma_i)_m}{(\gamma_\ell)_{m-1}}-1\right\|>tol_s,\ \left\|\frac{(R_i)_m}{(R_\ell)_{m-1}}-1\right\|>tol_s$	×
γ stability	$\left\|\frac{(\gamma_i)_m}{(\gamma_\ell)_{m-1}}-1\right\|<tol_s,\ \left\|\frac{(R_i)_m}{(R_\ell)_{m-1}}-1\right\|>tol_s$	□
R stability	$\left\|\frac{(\gamma_i)_m}{(\gamma_\ell)_{m-1}}-1\right\|>tol_s,\ \left\|\frac{(R_i)_m}{(R_\ell)_{m-1}}-1\right\|<tol_s$	*
Full stability	$\left\|\frac{(\gamma_i)_m}{(\gamma_\ell)_{m-1}}-1\right\|<tol_s,\ \left\|\frac{(R_i)_m}{(R_\ell)_{m-1}}-1\right\|<tol_s$	○

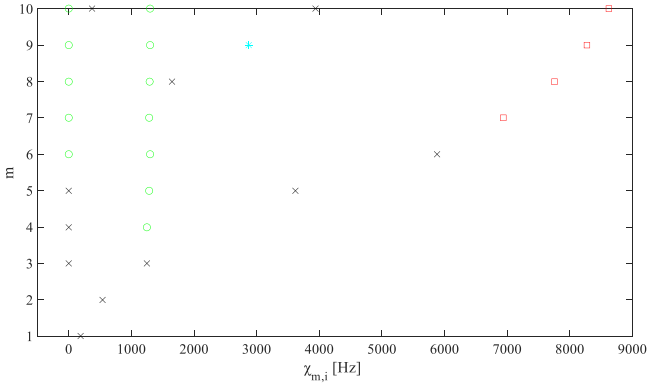

Fig. B1. Θ_F stability plot example, identified stable and unstable solutions, marked according to Table. B.1.

$$\mathbf{a}=[\,a_0\quad\ldots\quad a_i\quad\ldots\quad a_{m-1}\,]^T,\mathbf{b}=[\,b_0\quad\ldots\quad b_i\quad\ldots\quad b_{m-1}\,]^T;$$
$$\mathbf{q}=\left[\,(\omega_{N_X})^{-m}\quad\ldots\quad(\omega_{N_X})^{\ell-m}\quad\ldots\quad(\omega_{N_X})^{-1}\,\right]^T\in\Re^m;\tag{38}$$
$$\tilde{\mathbf{a}}=diag(\mathbf{q})\cdot\mathbf{a},\quad\tilde{\mathbf{b}}=diag(\mathbf{q})\cdot\mathbf{b}\,.$$

From Eq. (37), in compact form:

$$[\mathbf{C}\quad-\mathbf{D}]\cdot\begin{bmatrix}\tilde{\mathbf{a}}\\ \tilde{\mathbf{b}}\end{bmatrix}=\mathbf{L};$$
$$\tilde{\mathbf{a}}=[\,\tilde{a}_0\quad\ldots\quad\tilde{a}_i\quad\ldots\quad\tilde{a}_{m-1}\,]^T,\tilde{\mathbf{b}}=[\,\tilde{b}_0\quad\ldots\quad\tilde{b}_i\quad\ldots\quad\tilde{b}_{m-1}\,]^T,$$
$$\mathbf{C}=\begin{bmatrix}1&\ldots&u_1^{m-1}\\ \ldots&\ldots&\ldots\\ 1&\ldots&u_{N_X}^{m-1}\end{bmatrix},\quad\mathbf{D}=\begin{bmatrix}\Delta\Theta_1&\ldots&\Delta\Theta_1\cdot u_1^{m-1}\\ \ldots&\ldots&\ldots\\ \Delta\Theta_{N_X}&\ldots&\Delta\Theta_{N_X}\cdot u_{N_X}^{m-1}\end{bmatrix},\tag{39}$$
$$\mathbf{L}=\left[\,\Delta\Theta_1\cdot u_1^m\quad\ldots\quad\Delta\Theta_{N_X}\cdot u_{N_X}^m\,\right]^T.$$

The $2{\cdot}m$ $\tilde{\mathbf{a}}$, $\tilde{\mathbf{b}}$ unknown complex coefficients can be obtained by least squares solving Eq. (39) by means of a singular value decomposition (SVD) based technique, so that from Eq. (38) $\mathbf{a}=(diag(\mathbf{q}))^{-1}\cdot\tilde{\mathbf{a}}$, $\mathbf{b}=(diag(\mathbf{q}))^{-1}\cdot\tilde{\mathbf{b}}$ results as well. Since the solution can be found with respect to any m assumed value, it results that $\mathbf{a}=(\mathbf{a})_m$, $\mathbf{b}=(\mathbf{b})_m$. The same iterative approach previously adopted in Section 3.1.2, based on the evaluation of the stability of $(\mathbf{a})_m$, $(\mathbf{b})_m$ solution is proposed herein. For any $m=1,2,3,\ldots,m_{\max}$, the system $(\mathbf{z})_m$ poles can be evaluated from $(\mathbf{b})_m$ as the m zeros of the following polynomial function:

$$z^m+z^{m-1}\cdot b_{m-1}+\ldots+b_0=0.\tag{40}$$

System $(\mathbf{R})_m$ residues can be evaluated from $(\mathbf{z})_m,(\mathbf{a})_m$ as follows:

$$R_\ell=\lim_{j\cdot\omega\to z_\ell}\left[\sum_{i=1}^{m}\frac{R_i}{j\omega-z_i}\cdot(j\cdot\omega-z_\ell)\right]=\frac{\sum_{i=0}^{m-1}a_i\cdot(z_\ell)^i}{\prod_{\substack{i=1\\ i\neq\ell}}^{m}(z_\ell-z_i)}.\tag{41}$$

The parameters associated to the i-th hysteretic Kelvin element can be identified from Eq. (33):

$$\beta_i=1/R_i,\quad E_i=-z_i/R_i;\quad i=1\ldots m\,.\tag{42}$$

The identified hysteretic elements being stable with respect to different m values can be selected as the constituents of the hysteretic SLS model, while the other identified hysteretic elements, only resulting from the computational evaluation, can be discarded. The stability approach used in Section 3.1.2, detailed in Appendix B, is adopted, making it possible to automatically or manually select stable solutions taking into account user defined tolerance values.

As a matter of example, the $\Theta_H(j\cdot\omega)$ identification results obtained with respect to the simulated measurements from the (L) model case and the Θ_F identified model are presented, $m_{\max}=10$. The stabilization diagram is shown in Fig. 8: a single hysteretic SLS element stable solution is found starting from $m=5$. The $N_H=1$ identified hysteretic SLS model contribution is reported in Table 4, and the $\Theta_F(j\cdot\omega)+\Theta_H(j\cdot\omega)$ model identified curve plot is shown in Fig. 7, showing that an excellent agreement with the reference model $\Theta(j\cdot\omega)$ curve plot is obtained.

4. Numerical validation of the identification procedure

The identification procedure is applied to three numerical test cases, whose model reference parameters are reported in Table 5. $N_X=10^4$ measurements are simulated from the reference models, in the $\Omega=[10^{-3},10^4]$ Hz frequency range, and numerically generated random noise, assuming a S/N = 90 dB signal to noise ratio, is added to simulated measurements with respect to (O) test case. Identification parameters are: (M) $D=10$, $m_{\max}=20$, (N) $D=4$, $m_{\max}=20$, (O) $D=4$, $m_{\max}=10$. The identified model results are reported in Table 5, and $\Theta(j\cdot\omega)$ curve plot estimates from the reference and the identified model are shown in Figs. 9–11: an excellent agreement of the identified models with respect to the (M-N) reference models were obtained, and a good agreement was also found with respect to the (O) reference model simulated measurements with noise.

5. Experimental test case applications

Two BS1 and BS2 polymeric composite material beam specimens are experimentally tested in flexural forced vibration response condition by means of a TA Instruments DMAQ800 system, operating at T = 35 °C in the multi-frequency and strain control experimental mode with clamped-sliding boundary conditions, $N_X=202$, $\Omega=[10^{-2},2{\cdot}10^2]$ Hz. The maximum strain value of (0.05 ± 0.01)% was maintained constant during the measurement test. The material of the (BS1) specimen is obtained by mixing a commercially available ethyl cyanoacrylate polymeric resin and an environmentally sustainable steel powder obtained from recycled machining waste chip. The material of the (BS2)

specimen is obtained by mixing a commercially available epoxy dual component resin material Loxeal 31–10® and recycled carbon fibers. BS1 and BS2 specimen data are reported in Table 6.

Since BS1, BS2 specimen material is not homogeneous, the identification of the equivalent homogenized material model is here taken into account. A calibration procedure, proposed by the authors in previous works [4,15]. is applied to the test measurements in order to take into account of the dynamic contribution of the instrument frame, and of the inertial contribution of the distributed mass of the beam and of the moving mass of the instrument force measuring system. $E(j\omega_k),\ \omega_k \in \Omega$ discrete material estimates from measurement data are plotted in Figs. 12,13.

The BS1, BS2 optimal extended SLS model was obtained by fitting experimental data with the identification procedure described in Section 3 and in Appendix B. Identification parameters are: (BS1) $D = 10,\ m_{\max} = 10$ for $\Theta_F(j\omega)$ and $m_{\max} = 25$ for $\Theta_H(j\omega)$, (BS2) $D = 10,\ m_{\max} = 20$ for $\Theta_F(j\omega)$ and $m_{\max} = 25$ for $\Theta_H(j\omega)$. Extended SLS models are reported in Table 7 and the $E(j\omega) = (\Theta_F(j\omega) + \Theta_H(j\omega))^{-1}$ continuous extended SLS model curve fits are shown in Figs. 12,13 and compared to experimental data.

A SLS model was identified by means of the procedure previously presented by these authors [4], and the results are reported in Table 8 and Figs. 12–13. The identified model was compared to the optimal extended material model fit plots.

From the identified models, E_0 is estimated from Eq. (A.7) and τ_c creep relaxation time is estimated by applying the procedure described in Appendix A and these results are also reported in Tables 7 and 8.

6. Conclusions

A procedure for the non-parametric identification of the extended SLS model of the material of an experimentally tested beam specimen was proposed in this work. The model takes into account of the equivalent elastic and viscous properties of the material under investigation, in a wide dynamical frequency range, from the quasi-static behavior (relaxation response) to the low to high frequency vibrational behavior.

The identification technique proposed in this work is non-parametric, since the N_F optimal number of fractional Kelvin elements is assumed as unknown but can be obtained as a result at the end of the identification procedure. The technique is mainly based on an algebraic approach, leading to a numerically well-conditioned linear systems of equations in the frequency domain, to be solved by least square standard SVD procedures, and on the automatic or semi-automatic evaluation of stabilization diagrams in order to find the N_F optimal model order.

The SLS model was also extended to take into account of the material hysteretic behavior, typically occurring at medium to high test frequencies, in order to better fit test data when the contribution of SLS and fractional SLS model elements appears to be ineffective, but a non-physical, non-causal material model result and such result may not be acceptable in some contexts.

The identification procedure was tested with respect to some numerically generated test data with simulated noise, and results showed that the procedure was effective in all of the example cases taken into consideration. The procedure is also efficient, since it does not require computationally expensive numerical nonlinear optimization procedures, but it only deals with the solution of some low order over-determined systems of linear equations.

Some experimental test cases dealing with non-conventional composite materials, quite common in some modern engineering applications, are proposed, showing that a good model fit in the frequency domain can be obtained with a limited number of extended SLS material model elements and that material creep relaxation can also be effectively estimated from the identified model. Poor results obtained by identifying these same experimental data test sets by assuming a SLS Kelvin model are reported to justify the proposed identification of an extended SLS model.

CRediT authorship contribution statement

Stefano Amadori: Experimentation, Analysis, Writing – original draft preparation, **Giuseppe Catania**: Conceptualization, Methodology, Writing, Reviewing, Supervision.

Declaration of Competing Interest

The authors declare that they have no known competing financial interests or personal relationships that could have appeared to influence the work reported in this paper.

Data Availability

Data related to simulated tests are shown in the paper tables. Experimental test data are available on request.

Acknowledgements

Technical support from Andrea Zucchini, Danilo Persici from Marzocchi Pompe S.p.A., Italy, Casalecchio di Reno, Italy, and from Massimo Penatti and Alessandra Maino from Loxeal s.r.l. Italy, is kindly acknowledged.

Appendix A. Creep relaxation time and damping ratio estimate

From Eq. (8), $\varepsilon_i(t)$ strain output response of the i-th element of a N order fractional SLS material model to a σ_0 stress step input, assuming the Caputo fractional derivative definition holds, is [27,44,48]:

$$\begin{aligned} &\sigma(t) = E_i \cdot \left(\varepsilon_i(t) + \frac{\beta_i}{E_i} \cdot \frac{\partial^{\alpha_i}}{\partial t^{\alpha_i}} \varepsilon_i(t) \right) = \sigma_0 \ ; \quad \tau_i = \frac{\beta_i}{E_i} \\ &\varepsilon_i(t) = \frac{\sigma_0}{E_i} \cdot \left(1 - M_{\alpha_i} \left(\left(-\frac{t}{\tau_i} \right)^{\alpha_i} \right) \right) \end{aligned} , \tag{A.1}$$

where $M_{\alpha_i}()$ is the Mittag-Leffler function [48]:

$$M_{\alpha_i}(z) = \sum_{k=0}^{\infty} \frac{z^k}{\Gamma(k \cdot \alpha_i + 1)} \underset{\alpha_i = 1}{=} \exp(z), \tag{A.2}$$

where $\Gamma()$ is the gamma function. The total $\varepsilon(t)$ strain output response is:

$$\varepsilon(t) = \sum_{i=1}^{N} \varepsilon_i(t) = \sigma_0 \cdot \sum_{i=1}^{N} \left[\frac{1}{E_i} \cdot \left(1 - M_{\alpha_i} \left(\left(-\frac{t}{\tau_i} \right)^{\alpha_i} \right) \right) \right] \cdot \tag{A.3}$$

If a N order SLS material model is taken into account, $\alpha_i = 1,\ \forall i$ and Eq. (A.4) holds:

$$\varepsilon(t) = \sum_{i=1}^{N} \varepsilon_i(t) = \sigma_0 \cdot \sum_{i=1}^{N} \frac{1}{E_i} \cdot \left(1 - \exp\left(-\frac{t}{\tau_i} \right) \right). \tag{A.4}$$

The τ_c creep relaxation time can be defined as follows:

$$\varepsilon(t = \tau_c) = 0.95 \cdot \varepsilon(t \to \infty) = 0.95 \cdot \frac{\sigma_0}{E_0}, \tag{A.5}$$

or:

$$E_0 \cdot \sum_{i=1}^{N} \left[\frac{1}{E_i} \cdot \left(1 - M_{\alpha_i} \left(\left(-\frac{\tau_c}{\tau_i} \right)^{\alpha_i} \right) \right) \right] = 0.95 \quad , \tag{A.6}$$

where:

$$E_0{}^{-1} = \left| \sum_i E_i^{-1} \right|. \tag{A.7}$$

As an example, Fig. A1 shows how τ_c can be estimated from the (A1) material example case (Table A1).

Free vibration $v(t)$ response of a slender uniform, homogeneous beam specimen made of a N-elements SLS material, normal boundary conditions at the beam ends [2,3], excitation and response at the same axial position, can be analytically expressed as:

$$v(t) = \sum_{i=1}^{\infty} C_i \cdot \exp(\lambda_i \cdot t) = \sum_r \Delta v_r(t) \quad , \tag{A.8}$$

where an exponentially decreasing harmonic function $\Delta v_r(t)$ results from the contribution of any occurring $(\lambda_r,\ \lambda_r^*),\ \ (C_r,\ C_r^*)$ complex conjugate pairs in $v(t)$:

$$\begin{aligned} &\Delta v_r(t) = C_r e^{\lambda_r t} + C_r^* e^{\lambda_r^* t} = \gamma_r \cdot \exp(-\eta_r \cdot \omega_{n_r} \cdot t) \cdot \sin\left(\omega_{n_r} \cdot \sqrt{1 - \eta_r^2} \cdot t + \varphi_r \right) \\ &\omega_{n_r} = |\lambda_r|,\ \ \eta_r = -\frac{\Re(\lambda_r)}{|\lambda_r|},\ \gamma_r = |C_r|,\ \ \varphi_r = \arg(C_r) \end{aligned} \quad . \tag{A.9}$$

It results that η_r damping factors vary with respect of the assumed material order and parameters, and also with respect to the beam specimen geometry and boundary conditions. The beam flexural FRF between $\widehat{F}$ transverse excitation and $\widehat{v}$ transverse displacement can be expressed by means of the modal approach [3,15]:

$$\begin{aligned} &\frac{\widehat{v}}{\widehat{F}}(\omega) = \sum_{i=1}^{\infty} \frac{\psi_i}{(j \cdot \omega)^2 + k_i^2 \cdot \frac{\omega_0^2}{\Xi(\omega)}} \simeq \sum_{i=1}^{nm} \frac{\psi_i}{(j \cdot \omega)^2 + k_i^2 \cdot \frac{\omega_0^2}{\Xi(\omega)}} \\ &\Xi(j \cdot \omega) = \sum_{i=1}^{N} \frac{E_0 / \beta_i}{j \cdot \omega + \frac{E_i}{\beta_i}} = E_0 \cdot \Theta(j \cdot \omega) \end{aligned} \quad , \tag{A.10}$$

where nm is the number of modal terms approximating $\widehat{v}/\widehat{F}(\omega)$ when $\omega \in [0, \omega_{\max}]$ is assumed, k_i and $\psi_i$result from the system solution by assuming $\Xi(\omega) = 1$ [2,3]. The ω_0 circular frequency, specimen related, constant value depends on the beam geometry, E_0 and the material density.

It must be observed that for a N order SLS material model, Eq. (8), $\Xi(j \cdot \omega)$ can be expressed by means of the ratio of two polynomial functions [4]:

$$\Xi(j \cdot \omega) = \frac{a_{N-1} \cdot (j \cdot \omega)^{N-1} + . + a_1 \cdot (j \cdot \omega) + a_0}{(j \cdot \omega)^N + b_{N-1} \cdot (j \cdot \omega)^N + . + b_1 \cdot (j \cdot \omega) + b_0}. \tag{A.11}$$

From Eqs. (A.10,A.11):

$$\begin{aligned} &\frac{\psi_i}{(j \cdot \omega)^2 + k_i^2 \cdot \omega_0^2 \cdot \frac{1}{\Xi(\omega)}} = \frac{\psi_i}{(j \cdot \omega)^2 + k_i^2 \cdot \omega_0^2 \cdot \frac{(j \cdot \omega)^N + b_{N-1} \cdot (j \cdot \omega)^{N-1} + . + b_0}{a_{N-1} \cdot (j \cdot \omega)^{N-1} + . + a_0}} = \frac{\psi_i \cdot \left(a_{N-1} \cdot (j \cdot \omega)^{N-1} + . + a_0 \right)}{(j \cdot \omega)^2 \cdot \left(a_{N-1} \cdot (j \cdot \omega)^{N-1} + . + a_0 \right) + k_i^2 \cdot \omega_0^2 \cdot \left((j \cdot \omega)^N + b_{N-1} \cdot (j \cdot \omega)^{N-1} + . + b_0 \right)} = \\ &\frac{c_{i,N-1} \cdot (j \cdot \omega)^{N-1} + . + c_{i,1} \cdot (j \cdot \omega) + c_{i,0}}{(j \cdot \omega)^{N+1} + . + d_{i,1} \cdot (j \cdot \omega) + d_{i,0}} = \sum_{s=1}^{N+1} \frac{R_{i,s}}{j \cdot \omega - p_{i,s}} \end{aligned} \tag{A.12}$$

The $\eta_{i,s}$ damping ratio values can be estimated from $p_{i,s}$ poles as follows [3]:

$$\eta_{i,s} = -\frac{\mathrm{Re}(p_{i,s})}{\omega_{n_{i,s}}}, \quad \omega_{n_{i,s}} = |p_{i,s}|, \tag{A.13}$$

where any $p_{i,s}$, $p_{i,s}^*$ complex conjugate pair is associated to $\eta_{i,s}$, $\omega_{n_{i,s}}$ values, while real $p_{i,s}$ poles are associated to $\eta_{i,s} = 1$.

Eq. (A.10) results as the sum of rational functions and a partial fraction form results as well:

$$\frac{\widehat{\nu}}{\widehat{F}}(\omega) \simeq \sum_{i=1}^{nm} \frac{c_{i,N-1}\cdot(j\cdot\omega)^{N-1} + . + c_{i,1}\cdot(j\cdot\omega) + c_{i,0}}{(j\cdot\omega)^{N+1} + . + d_{i,1}\cdot(j\cdot\omega) + d_{i,0}} = \sum_{i=1}^{nm}\sum_{s=1}^{N+1} \frac{R_{i,s}}{j\cdot\omega - p_{i,s}} \ , \tag{A.14}$$

so that Eq. (A.14) also results as the ratio of polynomial functions, where the polynomial order of the denominator is greater than the polynomial order of the numerator, so that a partial fraction form holds:

$$\begin{aligned} &\frac{\widehat{\nu}}{\widehat{F}}(\omega) \simeq \frac{\widetilde{c}_0 + \widetilde{c}_1\cdot(j\cdot\omega) + . + \widetilde{c}_r\cdot(j\cdot\omega)^r + .}{\widetilde{d}_0 + \widetilde{d}_1\cdot(j\cdot\omega) + . + \widetilde{d}_s\cdot(j\cdot\omega)^s + .} = \sum_i \frac{R_i}{j\cdot\omega - p_i}, \\ &\eta_i = -\frac{\mathrm{Re}(p_i)}{|p_i|}, \quad \omega_{n_i} = |p_i|. \end{aligned} \tag{A.15}$$

An equivalent $\widehat{\nu}/\widehat{F}(\omega)$ FRF expression can be obtained as well by adopting a different approach [4]. From the Euler-Bernoulli homogeneous, uniform beam, with normal boundary conditions, the equation of motion in the frequency domain is obtained:

$$\frac{\partial^4}{\partial\xi^4}\widehat{\nu}(\xi,\omega) - z^4(\omega)\cdot\widehat{\nu}(\xi,\omega) = 0, \ \mathrm{z} = \sqrt[4]{\frac{\omega^2}{\omega_0^2\cdot\Xi(\omega)}} = \mathrm{z}(\omega,\omega_0), \ \omega_0 = \sqrt{\frac{E_0\cdot I}{\rho\cdot S\cdot L^4}}; \tag{A.16}$$

where $\xi = x/L$ refers to the normalized displacement, L to the beam length, ρ to the density, S to the section area, I to the section moment. The $\widehat{\nu}(\xi,\omega)$ solution that satisfies Eq. (A.16) is:

$$\widehat{\nu}(\xi,\omega) = C_1\cdot\sin(z\cdot\xi) + C_2\cdot\cos(z\cdot\xi) + C_3\cdot\sinh(z\cdot\xi) + C_4\cdot\cosh(z\cdot\xi) \tag{A.17}$$

Taking into account of the following boundary conditions, being consistent with a typical test measurement architecture: clamped beam at one end ($\xi = 0$), $T = -F$ shear and null M moment at the opposite beam end ($\xi = 1$), the terms C_1, C_2, C_3, C_4 terms from Eq. (A.17) can be obtained by imposing the following conditions, agreeing the previously cited boundary conditions:

$$\begin{aligned} &\widehat{\nu}(0,\omega) = 0 \ , \ \frac{1}{L}\cdot\frac{\partial}{\partial\xi}\widehat{\nu}(0,\omega) = 0 \ , \\ &\frac{E_0\cdot I\cdot\Xi(\omega)}{L^2}\cdot\frac{\partial^2}{\partial\xi^2}\widehat{\nu}(1,\omega) = 0 \ , \ \frac{E_0\cdot I\cdot\Xi(\omega)}{L^3}\cdot\frac{\partial^3}{\partial\xi^3}\widehat{\nu}(1,\omega) = -F. \end{aligned} \tag{A.18}$$

The resulting response function at $\xi = 1$ end is:

$$\begin{aligned} &\frac{\widehat{\nu}}{\widehat{F}}(j\cdot\omega) = \frac{1}{m_B\cdot\omega_0^{0.5}\cdot\omega^{1.5}\cdot[\Xi(j\cdot\omega)]^{0.25}}\cdot\left(\frac{\sin z\cdot\cosh z - \sinh z\cdot\cos z}{1 + \cos z\cdot\cosh z}\right) = \frac{1}{m_B\cdot\omega_0^{0.5}}\cdot\Phi\left(\omega_0 j\cdot\omega\right), \\ &\Phi\left(\omega_0 j\cdot\omega\right) = m_B\cdot\omega_0^{0.5}\cdot\frac{\widehat{\nu}}{\widehat{F}} = \frac{\sin(z(\omega_0,\omega))\cdot\cosh(z(\omega_0,\omega)) - \sinh(z(\omega_0,\omega))\cdot\cos(z(\omega_0,\omega))}{\omega^{1.5}\cdot[\Xi(j\cdot\omega)]^{0.25}\cdot(1 + \cos(z(\omega_0,\omega))\cdot\cosh(z(\omega_0,\omega)))}, \end{aligned} \tag{A.19}$$

where m_B is the total mass of the beam. It should be outlined that $\widehat{\nu}/\widehat{F}(\omega)$ from Eq. (A.19) corresponds to the exact solution, according to the model assumptions. Moreover, it also results that, from Eqs. (A.14,A.19):

$$\frac{\widehat{\nu}}{\widehat{F}}(\omega\to\omega_{n_r}) = \frac{1}{m_B\cdot\omega_0^{0.5}}\cdot\Phi\left(\omega_{0,}\omega\right) \simeq \frac{R_r}{j\cdot\omega - p_r} + \frac{R_r^*}{j\cdot\omega - p_r^*} \ , \tag{A.20}$$

and:

$$\Phi(\omega_0,\omega\to\omega_{n_r}) \simeq \frac{\widetilde{R}_r}{j\cdot\omega - p_r} + \frac{\widetilde{R}_r^*}{j\cdot\omega - p_r^*}, \quad \widetilde{R}_r = R_r\cdot m_B\cdot\sqrt{\omega_0} \ , \tag{A.21}$$

where $\omega_{n_r} = |p_r|$ is the natural frequency of a beam vibrational mode associated to a complex conjugate pole pair.

Starting from $\widehat{\nu}/\widehat{F}(\omega_k)$, $\omega_k \in \Omega$ measurement range from a known beam specimen, many numerical identification techniques [20], some developed by these authors in previous [3,15], can be employed to identify p_r, R_r parameters from Eq. (A.20), so that ω_{n_r}, η_r values can be found as well.

Since ω_{n_r}, η_r are expected to vary with respect to $\Xi(\omega)$ material model and to the beam geometry, E_0, ρ values only affecting m_B, ω_0 values, the pole identification technique can be iteratively applied from a $\Phi(\bar{\omega}_0,\omega_k)$, $\omega_k \in \Omega$ discrete set of analytically computed values at different $\bar{\omega}_0$ values, so that identified ω_{n_r} circular frequencies may assume any value in a known range. The η_r values obtained by applying the previously defined identification technique are thus associated to ω_{n_r} frequency value.

This same procedure can be used to estimate $\eta(\omega) = \eta_r(\omega_{n_r})$ for a beam specimen made of a material following a fractional SLS material model. It should be outlined that in this case Eq. (A.14) does not hold anymore, since $\widehat{\nu}/\widehat{F}(\omega)$ results as the ratio of pseudo-polynomial functions where the

exponent associated to each term of these functions is not expected to be integer anymore. By using Eq. (A.14) to approximately fit $\widehat{\nu}/\widehat{F}(\omega)$ and $\Phi(\omega_0, \omega)$, $\eta(\omega)$ estimates can be obtained for beam specimens made of a material following a fractional SLS material model. Fig. A2 refer to $\eta(\omega)$ identified estimate results related to example case (A1).

Appendix B. Non-parametric material model identification by the stability diagram approach

From $\Theta_k = \Theta(j\omega_k),\ \omega_k \in \Omega$ discrete measurement set and from Eqs. (10, 12, 20), assuming a N_F order fractional SLS model:

$$\Theta\left(q_k = (j\cdot\omega_k)^{\frac{1}{D}}\right) = \Theta_k,$$
$$\Theta_k = \sum_{i=1}^{N_F} \frac{1}{E_i + (j\cdot\omega_k)^{\frac{n_i}{D}}\cdot\beta_i} = \sum_{i=1}^{N_F} \frac{R_i}{q_k^{n_i} + \gamma_i} = \sum_{i=1}^{N_F}\left(\sum_{s=1}^{n_i} \frac{r_{i,s}}{q_k - z_{i,s}}\right) = \sum_{\ell=1}^{m} \frac{r_\ell}{q_k - z_\ell}, \qquad k = 1...N_X, \tag{B.1}$$

where $N_F \in \mathbb{N}$, $D \in \mathbb{N}$, $E_i,\ \beta_i,\ R_i,\ \gamma_i \in \Re^+,\ n_i \in \mathbb{N};\ \ i = 1...N_F$ are the model parameters to be identified. From Eq. (26-29) $z_\ell \in (\mathbf{z})_m,\ \ r_\ell \in (\mathbf{r})_m$ poles and residues can be obtained with respect to any m value. The $\widetilde{\mathbf{z}}_i = [\widetilde{z}_{i,1}, ..., \widetilde{z}_{i,n_i}]^T \in (\mathbf{z})_m$, $\widetilde{\mathbf{r}}_i = [\widetilde{r}_{i,1}, ..., \widetilde{r}_{i,n_i}]^T \in (\mathbf{r})_m\ i = 1...(N_F)_m$ subsets belonging to the i-th fractional SLS element, fractional order $\alpha_i = n_i/D$, should satisfy Eq. (30). Taking into account of numerical and experimental noise, $\widetilde{\mathbf{z}}_i,\ \ \widetilde{\mathbf{r}}_i$ are required to satisfy the following inequality conditions:

$$\begin{aligned}
&\left|\frac{|\widetilde{z}_{i,1}|}{|\widetilde{z}_{i,s}|} - 1\right| \le tol_r, \qquad \left|\left|\arg\left(\frac{\widetilde{z}_{i,s-1}}{\widetilde{z}_{i,s}}\right)\right| - \frac{2\pi}{n_i}\right| \le tol_{ph} \\
&\left|\frac{|\widetilde{r}_{i,1}|}{|\widetilde{r}_{i,s}|} - 1\right| \le tol_r, \qquad \left|\left|\arg\left(\frac{\widetilde{r}_{i,s-1}}{\widetilde{r}_{i,s}}\right)\right| - \frac{2\pi}{n_i}\right| \le tol_{ph},\ s = 2, ., n_i. \\
&\left|\left|\arg(\widetilde{z}_{i,1})\right| - \frac{\pi}{n_i}\right| \le tol_{ph}, \quad \left|\arg\left(\frac{\widetilde{r}_{i,1}}{\widetilde{z}_{i,1}}\right)\right| - \pi\right| \le tol_{ph}
\end{aligned} \tag{B.2}$$

tol_r and tol_{ph} tolerance values are associated to the experimental and numerical noise of the specific identification test case considered. The α_i fractional exponents, E_i average moduli and β_i average viscous coefficient values associated to the i-th fractional Kelvin element can be found from Eqs. (30,31). The $z_\ell \in (\mathbf{z})_m,\ \ r_\ell \in (\mathbf{r})_m$ solutions not satisfying Eq. (B.2) can be associated with a minimum order fractional Kelvin element if the following inequality conditions hold:

$$||\arg(z_\ell)| - \pi| \le tol_{ph}, \quad |\arg(r_\ell)| \le tol_{ph}, \tag{B.3}$$

and from Eq. (30,31):

$$E_i = \left|\frac{\widetilde{z}_{i,1}}{\widetilde{r}_{i,1}}\right|, \qquad \beta_i = \frac{1}{R_i} = \frac{E_i}{|\widetilde{z}_{i,1}|}, \qquad \alpha_i = \frac{1}{D}, \quad \gamma_i = \frac{E_i}{\beta_i}. \tag{B.4}$$

The $(N_F)_m$ order, fractional SLS model associated to the previously described m order fitting procedure is expected to include physical and nonphysical, computational components if high m values and noisy test measurements are taken into account.

For $m = 1, \ldots, m_{\max}$, the $(E_i,\ \beta_i,\ \alpha_i)_m$ solution stability properties are evaluated with respect to $(E_\ell,\ \beta_\ell,\ \alpha_\ell \equiv \alpha_i)_{m-1};\ \ \ell : \min_\ell(\left|(E_i)_m - (E_\ell)_{m-1}\right|)$. Stability conditions are reported in (Table B1).

The tol_s choice depends on the numerical and experimental noise associated to the identification procedure. The solutions related to $(E_i,\ \beta_i,\ \alpha_i)_m$ fractional element can be plotted in a stabilization diagram by means of the marker defined in Table B1 with respect to $(\chi_{m,i} = (|E_i/\beta_i|^{1/\alpha_i})_m, m)$ coordinates. Fig. B1 refers to a stabilization diagram example. Stable $(E_i,\ \beta_i,\ \alpha_i)_m$ solutions can be automatically or iteratively user selected from any column of stable solutions found in the stability plot. The total number of fully stable, selected choices, identifies the N_F unknown value.

The stabilization approach can be easily applied to the Θ_H hysteretic SLS model identification procedure as well.

References

[1] S. Amadori, G. Catania, Experimental identification of the constitutive model of viscoelastic non-standard materials, ASME Int. Mech. Eng. Congress Exposition Proc. (IMECE) (2016) 13, https://doi.org/10.1115/IMECE2016-66807.

[2] S. Timoshenko, D.H. Young, W. Weaver, Vibration Problems in Engineering, John Wiley & Sons Inc, 1974.

[3] S. Amadori, G. Catania, Robust identification of the mechanical properties of viscoelastic non standard materials by means of frequency domain experimental measurements, Compos. Struct. 169 (2017) 79–89, https://doi.org/10.1016/j.compstruct.2016.11.029.

[4] S. Amadori, G. Catania, Experimental identification of the material standard linear solid model parameters by means of dynamical measurements, J. Vib. Control 28 (23–24) (2022) 3688–3704, https://doi.org/10.1177/10775463211037151.

[5] W.N. Findley, J.S. Lai, K. Onaran, Creep and Relaxation of Nonlinear Viscoelastic Materials, Dover publications Inc, New York, 1989.

[6] R.L. Bagley, P.J. Torvik, On the fractional calculus model of viscoelastic behavior, J. Rheol. 30 (1) (1986), https://doi.org/10.1122/1.549887.

[7] T. Alfrey, Non-homogeneous stresses in visco-elastic media, Q. Appl. Math. 2 (1944) 113–119, https://doi.org/10.1090/qam/10499.

[8] T. Alfrey, Methods of representing the properties of viscoelastic materials, Q. Appl. Math. 3 (1945) 143–150, https://doi.org/10.1090/qam/12566.

[9] C. Zener, Elasticity and Anelasticity of Metals, University of Chicago Press, 1948.

[10] A.S. Nowick, B.S. Berry, Anelastic Relaxation in Crystalline Solids, Academic Press Inc, 1972.

[11] N.W. Tschoegl, The Phenomenological Theory of Linear Viscoelastic Behavior, Spinger, Berlin, 1989.

[12] L.E. Ramirez, C.F. Coimbra, A variable order constitutive relation for viscoelasticity, Ann. der Phys. 16 (2007) 543–552, https://doi.org/10.1002/andp.200751907-803.

[13] C.M.A. Vasques, R.A. Moreira, J.D. Rodrigues, R. Frias, Viscoelastic Damping Technologies-Part, I: modeling and finite element implementation, J. Adv. Res. Mech. Eng. 1 (2) (2010) 76–95.

[14] S. Amadori, G. Catania, Experimental identification of the material constitutive equation by means of forced sinusoidal excitation measurements, Proc. ISMA 2020 - Int. Conf. Noise Vib. Eng. USD 2020 - Int. Conf. Uncertain. Struct. Dyn. (2020) 2473–2486.

[15] S. Amadori, G. Catania, Material model robust identification procedure from dynamical measurements made on a flexible specimen-frame system, Compos. Struct. 269 (2021), 113981, https://doi.org/10.1016/j.compstruct.2021.113981.

[16] S. Amadori, G. Catania, An effective coating material solution and modeling technique for damping oriented design of thin walled mechanical components, Compos. Struct. 191 (2018) 251–267, https://doi.org/10.1016/j.compstruct.2018.02.034.
[17] B.J. Lazan, Damping in Materials and Members in Structural Mechanics, Pergamon, Oxford, 1968.
[18] H. Wittke, J. Olfe, K. Rie, Description of stress–strain hysteresis loops with a simple approach, Int. J. Fat. 19 (2) (1997) 141–149, https://doi.org/10.1016/S0142-1123(96)00059-X.
[19] B. Bahn, C. Hsu, Stress–strain behaviour of concrete under cyclic loading, Acids Mater. J. 95 (2) (1998) 178–193, https://doi.org/10.14359/7775.
[20] D.J. Ewins, Modal testing: theory, practice and applications, (2nd ed.), Research Studies Press Ltd., Hertfordshire, 2000.
[21] S. Sessa, N. Vaiana, M. Paradiso, L. Rosati, An inverse identification strategy for the mechanical parameters of a phenomenological hysteretic constitutive model, Mech. Syst. Signal Process. 139 (2020), 106622, https://doi.org/10.1016/j.ymssp.2020.106622.
[22] D.Y. Yvan, F. Morestin, N. Hamila, A hysteretic model for fiber-reinforced composites at finite strains: fractional derivatives, computational aspects and analysis, Comput. Mater. Sci. 181 (2020), 109716, https://doi.org/10.1016/j.commatsci.2020.109716.
[23] M.M. Javidan, S.H. Chun, J. Kim, Experimental study on steel hysteretic column dampers for seismic retrofit of structures, Steel Compos. Struct. 40 (2021) 495–509, https://doi.org/10.12989/scs.2021.40.4.495.
[24] G.S.W. Blair, Analytical and integrative aspects of the stress-strain problem, J. Sci. Instrum. 21 (1944) 80–84, https://doi.org/10.1088/0950-7671/21/5/302.
[25] R.C. Koeller, Application of fractional calculus to the theory of viscoelasticity, J. Appl. Mech. 51 (1984) 299–307, https://doi.org/10.1115/1.3167616.
[26] Y.A. Rossikhin, M.V. Shitikova, Application of fractional calculus to dynamic problems of linear and nonlinear hereditary mechanics of solids, Appl. Mech. Rev. 50 (1997) 15–67, https://doi.org/10.1115/1.3101682.
[27] F. Mainardi, Fractional Calculus and Waves in Linear Viscoelasticity: an Introduction to Mathematical Models, Imperial College Press, 2010, https://doi.org/10.1142/p614.
[28] R. Xiao, H. Sun, W. Chen, An equivalence between generalized Maxwell model and fractional Zener model, Mech. Mater. 100 (2016) 148–153, https://doi.org/10.1016/j.mechmat.2016.06.016.
[29] H. Xu, X. Jiang, Creep constitutive models for viscoelastic materials based on fractional derivatives, Comput. Math. Appl. 73 (2017) 1377–1384, https://doi.org/10.1016/j.camwa.2016.05.002.
[30] X. Su, D. Yao, W. Xu, A new method for formulating linear viscoelastic models, Int. J. Eng. Sci. 156 (2020), 103375, https://doi.org/10.1016/j.ijengsci.2020.103375.
[31] M. Caputo, F. Mainardi, A new dissipation model based on memory mechanism, Pure Appl. Geophys. 91 (1971) 134–147, https://doi.org/10.1007/BF00879562.
[32] S. Gerlach, A. Matzenmiller, On parameter identification for material and microstructural properties, GAMM-Mitt. 30 (2007) 481–505, https://doi.org/10.1002/gamm.200790028.
[33] J. Zhang, M.R. Christopher, Parameter identification of analytical and experimental rubber isolators represented by Maxwell models, Mech. Syst. Signal Process. 21 (2007) 2814–2832, https://doi.org/10.1016/j.ymssp.2007.02.007.
[34] D. Jalocha, A. Constantinescu, R. Nevière, Revisiting the identification of generalized Maxwell models from experimental results, Int. J. Solids Struct. 67 (2015) 169–181, https://doi.org/10.1016/j.ijsolstr.2015.04.018.
[35] B. Babaei, A. Davarian, K.M. Pryse, E.L. Elson, G.M. Genin, Efficient and optimized identification of generalized Maxwell viscoelastic relaxation spectra, J. Mech. Behav. Biomed. Mater. 55 (2015) 32–41, https://doi.org/10.1016/j.jmbbm.2015.10.008.
[36] T. Nguyen, J. Li, L. Sun, D. Tran, F. Xuan, Viscoelasticity modeling of dielectric elastomers by Kelvin Voigt-generalized Maxwell Model, Polymers 13 (2021) 2203, https://doi.org/10.3390/polym13132203.
[37] E.C. Levy, Complex-curve fitting, IRE Trans. Autom. Control, Vol. AC- 4 (1) (1959) 37–43, https://doi.org/10.1109/TAC.1959.6429401.
[38] T. Pritz, Five-parameter fractional derivative model for polymeric damping materials, J. Sound Vib. 265 (5) (2003) 935–952, https://doi.org/10.1016/S0022-460X(02)01530-4.
[39] A.L. Araújo, C.M. Soares, J. Herskovits, Optimal design and parameter estimation of frequency dependent viscoelastic laminated sandwich composite plates, Compos. Struct. 92 (2010) 2321–2327, https://doi.org/10.1016/j.compstruct.2009.07.006.
[40] K. Papoulia, V. Panoskaltsis, N. Kurup, I. Korovajchuk, Rheological representation of fractional order viscoelastic material models, Rheol. Acta 49 (2010) 381–400, https://doi.org/10.1007/s00397-010-0436-y.
[41] M. Sasso, G. Palmieri, D. Amodio, Application of fractional derivative models in linear viscoelastic problems, Mech. Time-Depend. Mat. 15 (2011) 367–387, https://doi.org/10.1007/s11043-011-9153-x.
[42] M.F. Costa, C. Ribeiro, Generalized fractional Maxwell model: Parameter estimation of a viscoelastic material, AIP Conf. Proc. 1479 (2012) 790, https://doi.org/10.1063/1.4756256.
[43] S.W. Katicha, G.W. Flintsch, Fractional viscoelastic models: master curve construction, interconversion, and numerical approximation, Rheol. Acta 51 (2012) 675–689, https://doi.org/10.1007/s00397-012-0625-y.
[44] S. Katsourinis, E. Kontou, Fractional viscoelastic for interconverting linear viscoelastic functions of various polymeric structures, Rheol. Acta 58 (2019) 307–309, https://doi.org/10.1007/s00397-019-01146-y.
[45] X. Su, D. Yao, W. Xu, Processing of viscoelastic data via a generalized fractional model, Int. J. Eng. Sci. 161 (2021), 103465, https://doi.org/10.1016/j.ijengsci.2021.103465.
[46] T. Pritz, Frequency power law of material damping, Appl. Acoust. 65 (2004) 1027–1036, https://doi.org/10.1016/j.apacoust.2004.06.001.
[47] D. Kapp, F. Weise, M. Ruderman, J. Reger, Fractional-order system identification of viscoelastic behavior: a frequency domain based experimental study, IEEE 16th International Workshop on Advanced Motion Control (AMC), Kristiansand, Nor. (2020) 153–160, https://doi.org/10.1109/AMC44022.2020.9244449.
[48] F. Mainardi, R. Gorenflo, 2008. Time-fractional derivatives in relaxation processes: a tutorial survey. arXiv: Mathematical Physics.